Research Article

Rajnish P. Modanwal, Madhur Gupta and Shailesh I. Kundalwal*

Effect of tunneling conductivity of CNTs on the EMI shielding effectiveness of nanocomposite in the C-band

https://doi.org/10.1515/jmbm-2024-0034
received September 04, 2024; accepted January 05, 2025

Abstract: In the present work, the electromagnetic interference (EMI) shielding effectiveness (SE) of carbon nanotube-reinforced nanocomposite (CNRC) is investigated by using an analytical approach. CNRC is composed of a polypyrrole matrix and carbon nanotubes (CNTs). The effect of the tunneling conductivity of CNTs on the EMI SE is studied quantitively, at different weight percentages (wt%) of CNTs, by varying the aspect ratio of CNTs, CNT-matrix interphase thickness, and waviness of CNTs. We observed that the SE is significantly influenced by the wt% of CNTs and the thickness of CNRC in the frequency range of 4.2–8.2 GHz (C-band). To support the theoretical investigations and understand the shielding mechanism of CNRC, a finite-element model is derived using commercially available software Ansys HFSS. The outcomes of both models are in good agreement. In addition, our investigation reveals that the electrical conductivity of CNRC is significantly improved with the increased wt% and aspect ratio of CNTs, as well as with increased interphase thickness. However, it degrades as the waviness of CNT increases. Our results suggest that the raised tunneling conductivity of CNTs improves the EMI SE of CNRC significantly. For the sake of greater clarity, the quantitative relative performance of the CNRC is also presented. Our foundational study highlights an opportunity to develop effective and lightweight CNT-based nanocomposites, which can be used in EMI SE applications.

Keywords: carbon nanotubes, polypyrrole, electromagnetic interference, shielding effectiveness, tunneling conductivity

Nomenclature

σ_N	Electrical conductivity of CNTs (S/m)
σ_m	Electrical conductivity of matrix (S/m)
σ_s	Electrical conductivity of tunneling distance of CNTs (S/m)
σ_{ND}	Electrical conductivity of extended CNTs (S/m)
σ_{NW}	Electrical conductivity of wavy CNTs (S/m)
σ	Electrical conductivity of CNRC (S/m)
σ_{Cu}	Electrical conductivity of copper (5.87×10^7 S/m)
σ_r	Relative conductivity of nanocomposite
s	Tunneling distance between nanoparticles (m)
a	Contact area of CNTs (m^2)
R_s	Resistance of tunneling distance between CNTs (Ω)
R_N	Resistance of CNTs (Ω)
R_{ND}	Effective electrical resistance (Ω)
R	Radius of CNTs (m)
l	Length of CNTs (m)
l_{eq}	Equivalent length of wavy CNTs (m)
f	Percentage of networked CNTs (%)
ϕ_p	Percolation threshold volume fraction
ϕ_{eff}	Effective volume fraction of effective CNTs
V_{ex}	Excluded volume of CNTs (m^3)
V	Volume of CNTs (m^3)
t	Interphase thickness (m)
u	Waviness factor
b	Thickness of shielding materials (m)
δ	Skin depth (m)
d	Screen distance (m)
n	Frequency of electromagnetic waves (Hz)
Z_w	Wave impedance (Ω)
Z_s	Conductor impedance (Ω)

*** Corresponding author: Shailesh I. Kundalwal,** Applied and Theoretical Mechanics (ATOM) Laboratory, Department of Mechanical Engineering, Indian Institute of Technology Indore, Indore, 453552, India, e-mail: kundalwal@iiti.ac.in
Rajnish P. Modanwal: Applied and Theoretical Mechanics (ATOM) Laboratory, Department of Mechanical Engineering, Indian Institute of Technology Indore, Indore, 453552, India
Madhur Gupta: Applied and Theoretical Mechanics (ATOM) Laboratory, Department of Mechanical Engineering, Indian Institute of Technology Indore, Indore, 453552, India; Department of Metallurgical Engineering and Materials Science, Indian Institute of Technology, Mumbai, 400076, India

μ	Magnetic permeability (H/m)
μ_o	$4\pi \times 10^{-7}$ (H/m)
μ_r	Relative permeability of CNRC
f_c	Cut-off frequency (GHz)
p	Width of waveguide (m)
q	Thickness of waveguide (m)
c	Speed of light (m/s)

1 Introduction

During the past few decades, electromagnetic interference (EMI) has become a critical problem, which originates from the electromagnetic (EM) field created by electronic devices. The term EMI is defined as the emission of radiation from an electronic component, which affects the performance of its neighboring electronic components. Thus, the EMI is an offensive electronic wave, which disturbs the operation of other electronic devices and is detrimental to space applications. For example, in the aerospace industry, manufacturers explore all possible means to control the EMI during the design and development stages of payload components. A typical payload consists of numerous powerful components such as traveling-wave tube amplifiers, muxs, waveguide joints, isolators, antennas, and feeds. These powerful components emit large amounts of radiation when they are operational. Apart from these, numerous sensitive components such as receivers, pre-amplifiers, high-gain solid-state amplifiers, demuxs, and filters are also mounted on the payload. The radiation emitted from both powerful components and sensitive components results in their performance degradation [1,2]. A similar problem is also faced by electronic industries, especially in wireless and communication systems, such as the control panels of airplanes, mobile phones, and computer systems. In the case of these devices, EMI is the most dominant cause of malfunction [3,4]. Also, an excess of such radiation in the environment is hazardous to life [5–8]. Therefore, it is necessary to block EM emissions in order to increase the performance of electronic devices and eliminate their hazardous effects on living creatures. The EMI shielding effectiveness (SE) is one such powerful process that blocks EM emissions from electronic devices.

The major mechanisms for EMI attenuation include reflection, absorption, and multiple reflections. The primary mechanism of EMI SE is absorption, which requires the existence of electric or magnetic dipoles to interact with EM radiation. It changes according to the thickness of the materials. Materials with a high dielectric constant provide electric dipoles, while materials with high magnetic permeability provide magnetic dipoles for the EMI SE by absorption. Reflection is the secondary mechanism of EMI SE. For reflection, the material must possess mobile charge carriers such as electrons or holes interacting with EM radiation. However, it is found that multiple reflections may be neglected when the SE due to the absorption is ≥10 dB [9,10]. Over the past few decades, metallic materials such as metallic coating, metal oxides, metallic fibers, and metallic fillers have been widely used for EMI SE applications. Such metallic materials have inherent attributes such as conductivity, permeability, and permittivity [11–15]. However, metallic materials are quite heavy, require more servicing, and corrode easily. This limits their use in aerospace applications [16–20]. In order to overcome the drawbacks of conventional metallic shielding materials, numerous research studies are being conducted to obtain alternative lightweight shielding materials that can block EMI effectively.

Recently, polymer-based materials have attracted considerable attention from researchers due to their unique properties such as light weight, corrosion resistance, low cost, easy processability, thermomechanical, and other properties, and potential for easy synthesis using different techniques [21–28]. A large variety of conducting polymers such as polyaniline, polyphenylacetylene, polythiophene, and polypyrrole (PPy) are being used for the EMI shielding of devices [4,16,29]. Among them, PPy proves to be an attractive conducting polymer due to its good electrical conductivity (EC), simple processability, environmental stability, and incredible response in terms of EMI SE [30,31]. It is worth noting that PPy can also restrain EMI up to a lower frequency range, which is usually difficult in the case of conventional materials. However, PPy is not suitable for estimating EMI SE at a higher frequency range. Therefore, carbon nanotube (CNT)s are introduced within the PPy matrix in order to improve the conductivity of composite materials and make them suitable for use at a higher frequency range [32–34].

The introduction of CNTs, graphene, and boron nitride tubes has sparked a great deal of research about the prediction of their unique electrical, thermal, and mechanical properties [35–38]. Several research investigations have revealed that the incorporation of CNTs in the polymer matrix significantly improves the EC of the resulting nanocomposite. Furthermore, the alignment, dispersion, and concentration of CNTs in nanocomposites are critical factors that significantly influence the EMI SE of nanocomposites. These factors control the formation of conductive CNT networks within the matrix, which determine how effectively the composite can reflect, absorb, and dissipate EM waves. In contrast, CNTs alignment refers to how the nanotubes are oriented within the matrix, whether they are aligned in a specific direction or randomly dispersed.

An aligned CNT enhances directional conductivity and can improve EMI SE in specific directions, favoring reflection at higher frequencies. However, dispersion of CNTs refers to how uniformly the CNTs are distributed within the matrix material. Poor dispersion leads to agglomeration of CNTs that decreases the properties of nanocomposites, while a good dispersion ensures uniform EMI SE by creating consistent conductive networks, enhancing both SE due to reflection and absorption. Furthermore, CNT concentration is defined as the amount of CNTs incorporated into the matrix material. CNT concentration must be optimized to reach the percolation threshold and beyond, so that the EC and EMI SE both improve significantly [39,40]. Also, it was observed that the mechanical properties of nanocomposite are enhanced by the incorporation of CNTs in the polymer matrix [41–47]. For instance, Gahlout and Choudhary [33] experimentally evaluated the EC and SE of multiwalled CNT/PPy nanocomposites through the doping of 5-sulfoisophtalic acid monolithium salt. They found that the EC and EMI SE of the nanocomposite were enhanced due to the incorporation of CNTs in the matrix material. Liu and Wan [48] determined the EC and ferromagnetic behavior of PPy composites using a synthesized chemical method in the presence of *p*-dodecylbenzene sulfonic acid sodium salt and hydrochloric as a dopant. They found that the magnetic properties of the PPy composite showed ferromagnetic behavior. Further, they reported that the EC of the PPy composite is about 10 S/cm. Kaur and Dhawan [16] synthesized PPy nanoparticles by using the surfactant-directed chemical oxidation method. They predicted that the EC and EMI SE of PPy nanoparticles increase, even as the particle size of a PPy decreases. Ebrahimi and Gashti [32] fabricated multiwalled CNTs/silver/PPy nanocomposites *via* chemical deposition and ultraviolet (UV) reduction methods. They examined the electrical and EMI SE properties of fabricated nanocomposites. They reported that the EC and SE of MWCNT/silver/PPy nanocomposites improve *via* the UV reduction method, as compared to the chemical deposition method. Mohameed and Sundararaj [10] investigated the EMI SE and electrical resistivity of MWCNT and polypropylene. They found that the electrical resistivity of developed nanocomposites decreases as the volume fraction of MWCNTs increases. They estimated the SE by fabricating composite samples with different thicknesses and concentrations of MWCNTs. It was reported that the SE of nanocomposites increases with an increase in the sample thickness and concentration of MWCNTs. Liu *et al.* [24] determined the SE and electrical resistivity of CNT-reinforced carbon fiber/pyrolytic carbon composites. They observed that the electrical resistivity of nanocomposites diminished with an increase in the weight fraction of CNTs. They also concluded that the SE of nanocomposite increases with an increase in the weight fraction of CNTs.

The reviewed literature indicates that the addition of CNTs into the polymer matrix results in an increase in the EC and EMI SE of nanocomposites. This is attributed to the fact that the dispersion of electrically conductive CNTs in a polymer matrix results in the percolated conductive network of CNTs, which makes nanocomposites electrically conductive. Existing studies have proved that the incorporation of CNTs above the percolation threshold increases their conductive network density in a polymer matrix. This consequently increases the electrical properties of nanocomposites such as tangent of dielectric loss angle, dielectric breakdown, dielectric constant, and EC [49]. Among these properties, EC is the most important property, as higher EC can provide better SE of materials, according to a previous study [33].

Existing studies showed that the EC of nanocomposites is the function of the following parameters: (i) filler content, waviness, aspect ratio, size, orientation, surface energy of fillers; (ii) filler/matrix contact resistance and associated interphases thickness; and (iii) matrix surface energy [50–54]. Among these, the waviness of fillers, aspect ratio of fillers, and interphase thickness influence the EC of nanocomposites *via* a tunneling effect. Traditional conductive mechanisms rely on continuous, physically connected pathways, while tunneling conductivity involves quantum mechanical phenomena [19,55–58]. In contrast, traditional conductivity in nanocomposites is primarily achieved through direct contact between conductive fillers, where electrons move freely along continuous conductive pathways formed by physical connections between fillers. However, tunneling conductivity is defined as a phenomenon where electrons tunnel between CNTs that are not physically in contact but are close enough for quantum tunneling to occur. In contrast, when CNTs are dispersed in the polymer matrix, they form a network. In such a network, some of the CNTs are not in direct contact with others since they are separated by a small distance (nanometre range). Hence, electrons can move through a polymer medium known as tunneling conductivity [59–64]. In order to increase the EMI SE, a highly conductive material is required to attenuate EM radiation by reflection and absorption [4,32]. Therefore, the tunneling effect is a crucial mechanism for determining the EC of CNT-based nanocomposites. The review of the above literature on the CNT-based nanocomposite indicates that CNT is one of the most fascinating nanofiller materials, which can be used to improve the EMI SE response of materials. The literature review indicates that several researchers have

studied the SE of CNT-reinforced PPy nanocomposites [32,33,65–67]. However, to the best of current authors' knowledge, no research study has investigated the tunneling effect of CNTs accounting (i) the aspect ratio of CNTs, (ii) waviness of CNTs, and (iii) CNT-matrix interphase thickness on the SE of CNRC. This is indeed the motivation behind the current study. In this study, an analytical model is derived to investigate the EC of CNRC, which takes into consideration such parameters. Further, the impact of aspect ratio and waviness of CNTs as well as of interphase thickness on the percolation threshold is also studied. Further, the EMI SE of CNRC is estimated analytically by considering the tunneling effect of CNT in the PPy matrix within the C-band (4.2–8.2 GHz) region. We considered the C-band in the present work since it has numerous real-world applications. At present, many satellite communications transmissions occur in the C-band frequency range. Additionally, several Wi-Fi devices, weather radar systems, surveillance, 5G networks, and cordless telephones operate in the C-band frequency range [68,69]. The SE is calculated by changing the wt% of CNT as well as the sample thickness of CNRC.

2 Analytical and finite-element (FE) modeling of CNRC

2.1 Analytical modeling

In this section, the EC and EMI SE of CNRC are examined by developing an analytical model. A CNRC is composed of CNTs and PPy matrix by considering the rectangular representative volume elements (RVEs). All the analytical modeling is performed with the help of the MATLAB program [70–72]. Figure 1(a) represents the schematic diagram of CNRC reinforced with CNTs in the PPy matrix. In this analysis, we have restricted ourselves to a single RVE. The axial and transverse cross-sections of CNRC RVE are illustrated in Figure 1(b). The following assumptions were adopted in the current study:

- The cylindrical molecular structure of CNT may be treated as an equivalent solid cylinder fiber.
- CNTs are randomly distributed throughout the PPy matrix in order to create a conductive network.
- The composite is homogeneous throughout.

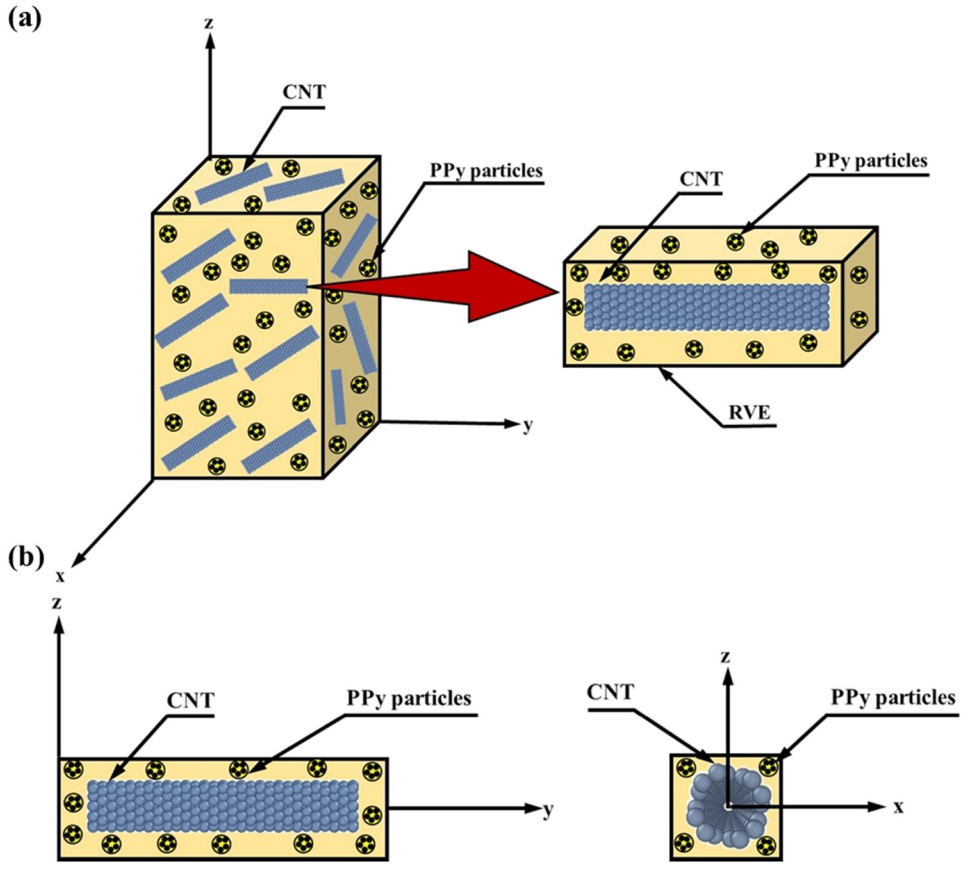

Figure 1: (a) Schematic representation of CNRC and (b) axial and transverse cross-sections of CNRC RVE.

- There is no slippage between the CNTs and the PPy matrix.

2.1.1 Simulation of EC

A theoretical model is proposed for the CNT-based nanocomposite by considering the tunneling gaps between the CNTs [73]. It is observed that the tunneling distance between two CNTs depends on the distance between one CNT and its neighboring CNTs. This approach is applied to determining the conductivity of nanocomposites, wherein electron tunneling is the chief mechanism. In this model, it is assumed that the tunneling distances are oriented along the x, y, and z directions and can be expressed as

$$\sigma_s = Y \exp(-Xs), \tag{1}$$

where s, X, and Y denote the distance between nanoparticles, characteristic tunneling distance, and constant parameter, respectively. If the distance between the nanoparticles is zero (*i.e.*, $s = 0$), then Y parameter can be considered as the conductivity of CNTs (σ_N). Hence, Eq. (1) can be modified as follows:

$$\sigma_s = \sigma_N. \tag{2}$$

Also, the value of X is suggested as 2, which presents accurate results compared to experimental data [73]. Finally, Eq. (1) can be rewritten as

$$\sigma_s = \sigma_N \exp(-2s). \tag{3}$$

Based on the percolation threshold, the curve of conductivity *versus* the volume fraction of nanocomposites can be divided into three parts, as shown in Figure 2. Part 1 represents the EC of the nanocomposites at a low volume fraction of CNTs, wherein conductive particles are not well connected to each other. Therefore, the electrical properties of composites are close to the EC of the matrix. Part 2 shows that the increased volume fraction of conductive particles generates a sudden increment in the EC of nanocomposites. This is due to the presence of sufficient fillers to form inter-particle connections between the conductive fillers. This critical volume fraction is called the percolation threshold. Beyond this percolation threshold, the further increment in the volume fraction of nanofillers leads to a dramatic increase in the EC. This is due to the dense network of nanofiller forms in the matrix, as shown in part 3 (Figure 2) [74,75].

Figure 3 demonstrates the in-plane contact between two adjacent CNTs. It is observed that as the wt% of CNT increases in the matrix, the separation distance between

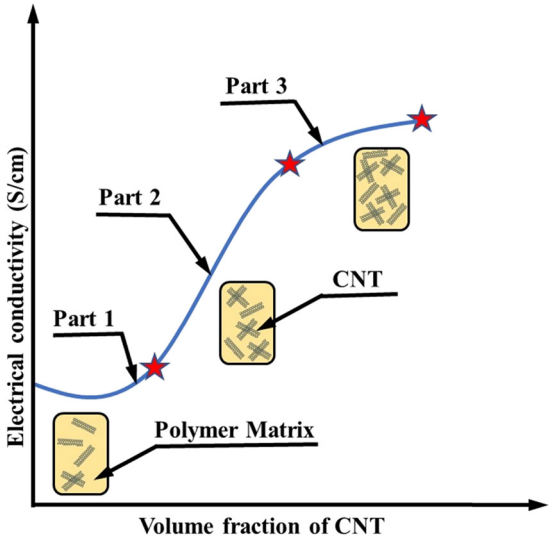

Figure 2: Description of three parts of the curve of composite conductivity *versus* filler volume fraction.

CNTs decreases. Subsequently, the formation of conductive networks begins. According to power law [60], tunneling distance can be expressed as

$$s = \frac{\alpha}{f^{\frac{1}{3}}}, \tag{4}$$

where f denotes the weight percentage of CNTs and α is a constant. The upper limit separation distance for CNTs in conductive networks is suggested as $s_c = 1.8$ nm [60]. Therefore, α can be approximately determined as

$$\alpha = s_c \phi_p^{\frac{1}{3}}. \tag{5}$$

However, due to the presence of van der Waals force between CNTs, these percolated CNTs continue to be in electrical rather than physical contact. Therefore, the thickness of the interphase can be expressed as

$$t = \frac{s}{2}. \tag{6}$$

Finally, combining Eqs. (4) and (5) into Eq. (6), the interphase thickness can be written as follows:

$$t = \frac{1}{2}\left(\frac{\phi_p}{f}\right)^{\frac{1}{3}} s_c. \tag{7}$$

The tunneling-type contact resistance between two CNTs is proposed by Simmons's derivation for electron tunneling. It can be expressed as

$$R_s = \frac{sh^2}{ae^2(2m\lambda)^{1/2}} \exp\left(\frac{4\pi s}{h}(2m\lambda)^{\frac{1}{2}}\right), \tag{8}$$

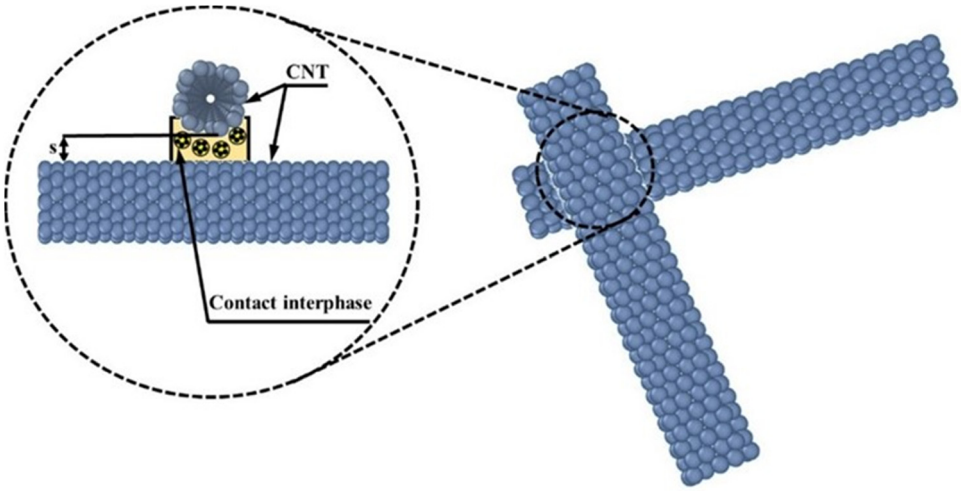

Figure 3: Contact configuration between two CNTs.

where λ is the potential barrier height (which is approximately 5.0 eV for CNTs dispersed in most polymers), m is the mass of an electron, e is the electric charge on the electron, a is the contact area of CNTs, and h is the plank constant. Therefore, the electrical resistance due to tunneling resistance can be written as

$$R_s = \frac{s}{a\sigma_s}. \tag{9}$$

It is to be noted that there are two types of conductive contact configuration formed between two CNTs (Figure 4). One conductive configuration is formed due to the overlapping of CNTs, as shown in Figure 4(a). For this conductive configuration, the contact area at the overlapping position is $4R^2$. Whereas, another conductive configuration is formed due to the in-plane contact configuration, as shown in Figure 4(b). For this conductive configuration, the contact area is equal to the cross-sectional area of nanotubes, *i.e.*,πR^2. Finally, an average contact area is determined by considering both configurations. This average contact area is approximately equal to $3R^2$ [61]. Hence, transforming Eq. (3) into Eq. (9), the resistance of tunneling distance between CNTs can be written as follows:

$$R_s = \frac{s}{a\sigma_N \exp(-2s)},$$

$$R_s = \frac{s}{3R^2\sigma_N \exp(-2s)}. \tag{10}$$

The effective electrical resistance can be defined as the sum of the resistance induced due to the CNTs and the tunneling distance between CNTs. Thus, effective electrical resistance can be expressed as

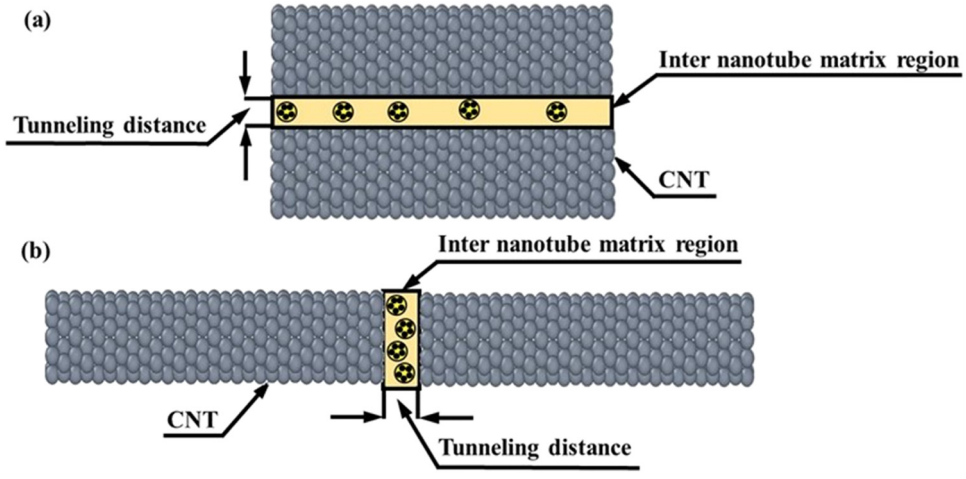

Figure 4: CNTs network dominated by (a) overlapping contact configuration and (b) in-plane contact configuration.

$$R_{ND} = R_N + R_s, \tag{11}$$

$$R_N = \frac{l}{\pi R^2 \sigma_N}, \tag{12}$$

$$R_{ND} = \frac{s}{3R^2\sigma_N \exp(-2s)} + \frac{l}{\pi R^2 \sigma_N}, \tag{13}$$

where l is the length, R is the radius of CNTs, and R_N is the resistance offered by CNTs. Based on Eq. (12), the conductivity of tunneling distance of CNTs can be written as

$$\sigma_{ND} = \frac{l_{ex}}{\pi (R_{ex})^2 R_{ND}}, \tag{14}$$

where l_{ex} denotes the length and R_{ex} denotes the radius of extended CNTs. The length of CNTs is much more than the tunneling distance. Therefore, l_{ex} is predicted as the length of CNTs. It is noted that the radius of extended CNTs does not change with tunneling distance. Thus, Eq. (14) can be re-expressed as

$$\sigma_{ND} = \frac{l}{\Pi R 2 R_{ND}}. \tag{15}$$

By changing Eq. (13) into Eq. (15), the EC of extended CNTs can be written as

$$\sigma_{ND} = \frac{l}{\Pi R 2 \left[\frac{s}{3R2\sigma N \exp(-2s)} + \frac{l}{\Pi R 2 \sigma N}\right]},$$

$$\sigma_{ND} = \frac{l\sigma_N}{\frac{s}{\exp(-2s)} + l}. \tag{16}$$

The above expression represents the EC of CNTs by considering the tunneling distance of CNTs. Furthermore, this calculated EC of CNTs can be used to develop a model to evaluate the EC of CNRC by considering the tunneling mechanism. The EC of CNTs-based nanocomposite can be determined by using the model derived by Deng and Zheng [59]. This model is developed by low loading of randomly distributed CNTs and can be expressed as

$$\frac{\sigma}{\sigma_m} = 1 + \frac{f}{3}\left[\frac{1}{\left(\frac{\sigma_3}{\sigma_m} - 1\right)^{-1} + H} + \frac{2}{\left(\frac{\sigma_1}{\sigma_m} - 1\right)^{-1} + \frac{(1-H)}{2}}\right], \tag{17}$$

where σ_1 and σ_3 denote the transverse and axial EC of CNTs, σ_m denotes the EC of the isotropic matrix, and H denotes the influence of the aspect ratio ($p = l/d$)

$$H(p) = \frac{1}{p^2 - 1}\left[\frac{p}{\sqrt{p^2 - 1}} \ln(p + \sqrt{p^2 - 1}) - 1\right]. \tag{18}$$

It is to be noted that the ratio of σ_3/σ_m is very large, and to date, there seems to be no measured value of σ_1 for CNTs. This is because the wavy CNTs have a curled graphite structure. Thus, it is assumed that the axial and transverse EC of CNTs would be similar to those of the graphite basal. In addition, $H(p)$ is a decreasing function of p. On the basis of this analysis, Eq. (17) can be expressed as

$$\frac{\sigma}{\sigma_m} = 1 + \frac{f}{3}\left[\frac{1}{\frac{\sigma_3}{\sigma_m} + H}\right]. \tag{19}$$

If the incorporation of CNTs within the nanocomposite increases, then it will lead to a situation wherein the percolation level of CNTs is exceeded. It is found that, after percolation, the CNTs would be electrically linked to form a conductive network, even though they would still not be physically connected to each other. At this stage, the above model should be modified and expressed as

$$\sigma = \sigma_m + \frac{f \phi_f \sigma_N}{3}, \tag{20}$$

where ϕ_f is the filler-weight fraction. Transforming Eq. (16) into Eq. (20), the generalized tunneling conductivity of CNT-based nanocomposite can be expressed as

$$\sigma = \sigma_m + \frac{fl\phi_f \sigma_N}{\frac{3s}{\exp(-2s)} + 3l}. \tag{21}$$

The above model represents the EC of CNT/PPy-based nanocomposites as a function of CNTs network properties. However, this model does not regard the influence of interphase and CNTs curvature on the conductivity, though these terms significantly affect the percolation threshold and the percentage of networked fillers.

A soft-core Sphero cylinder model is devolved in order to estimate the percolation in 3D fiber systems with the help of Monte Carlo simulations [76]. In this model, it is assumed that the number of objects per unit volume at percolation q_p is inversely proportional to the excluded volume of one of the objects and can be written as

$$q_p \propto \frac{1}{V_{ex}}. \tag{22}$$

If $\frac{R}{l} \to 0$, then the above proportionality becomes unity. Therefore, in the case of a very high aspect ratio of CNTs, the above expression can be written as

$$q_p = \frac{1}{V_{ex}}. \tag{23}$$

Since q_p is the number of objects per unit volume at percolation, the analytical solution for the volume-fraction of high aspect ratio fibers at the percolation threshold is often written as

$$\phi_p = \frac{V}{V_{ex}}, \tag{24}$$

where V and V_{ex} denotes the volume and excluded volume of CNTs, respectively. Excluded volume is defined as the volume in which the center of the same particle cannot be arrived at. The expression for the excluded volume can be written as

$$V_{ex} = \frac{32}{3}\pi R^3\left[1 + \frac{3}{4}\left(\frac{l}{R}\right) + \frac{3}{8\pi}\langle \sin(\theta)\rangle\left(\frac{l}{R}\right)^2\right], \tag{25}$$

$$V = \pi R^2 l + \frac{4\pi R}{3}, \tag{26}$$

where θ denotes the angle of inclination between two CNTs, and $\langle \sin(\theta)\rangle$ denotes the average value of $\sin(\theta)$. In the case of a random distribution of CNTs, $\langle \sin(\theta)\rangle = \frac{\pi}{4}$ [62]. Therefore, Eq. (22) can be expressed as

$$V_{ex} = \frac{32}{3}\pi R^3\left[1 + \frac{3}{4}\left(\frac{l}{R}\right) + \frac{3}{32}\left(\frac{l}{R}\right)^2\right], \tag{27}$$

$$V_{ex} = \frac{32}{3}\pi (R + t)^3\left[1 + \frac{3}{4}\left(\frac{l}{R + t}\right) + \frac{3}{32}\left(\frac{l}{R + t}\right)^2\right], \tag{28}$$

where t denotes the interphase thickness. In addition, the high aspect ratio of CNTs has the tendency to form waviness and reduce the effectiveness of conductivity. Figure 5 illustrates the transmission electron microscopy (TEM) image of CNTs. In this figure, we can clearly observe the sinusoidal curvature of CNT.

For mathematical modeling, we have considered both the straight and wavy CNT, as shown in Figure 6(a) and (b). Therefore, the waviness factor (u) can be defined as

$$u = \frac{l}{l_{eq}}, \tag{29}$$

where l_{eq} is the equivalent length of wavy CNTs vis-a-vis the straight CNTs. Finally, by combining Eqs. (26), (28), and (29) into Eq. (24), the percolation threshold, after considering the interphase thickness and waviness, can be expressed as follows:

$$V_{ex} = \frac{32}{3}\pi (R + t)^3\left[1 + \frac{3}{4}\left(\frac{l/u}{R + t}\right) + \frac{3}{32}\left(\frac{l/u}{R + t}\right)^2\right],$$

$$\phi_p = \frac{\Pi R^2 l + \left(\frac{4}{3}\right)\Pi R^3}{\frac{32}{3}\Pi (R + t)^3\left[1 + \frac{3}{4}\left(\frac{\frac{l}{u}}{R + t}\right) + \frac{3}{32}\left(\frac{\frac{l}{u}}{R + t}\right)^2\right]}. \tag{30}$$

Figure 7 depicts the CNTs with interphase thickness. In this figure, CNTs and their surrounding interphase are included. The CNT-matrix interphase thickness refers to the region between the CNT and the surrounding polymer matrix in a nanocomposite material [60]. This region has unique properties due to the interaction between the CNTs and the matrix, often resulting in a transition zone where the mechanical, electrical, and thermal properties differ from both the CNTs and bulk matrix. The EC of nanocomposite shows a direct dependency on the interphase thickness, and EMI SE shows a direct dependency on the EC of nanocomposite [4,78]. In contrast, both parameters increase with increases in the thickness of the interphase. Hence, to estimate the effective volume fraction of CNT, we assume the role of interphase and curvature of CNTs [60]. This equation can be written as

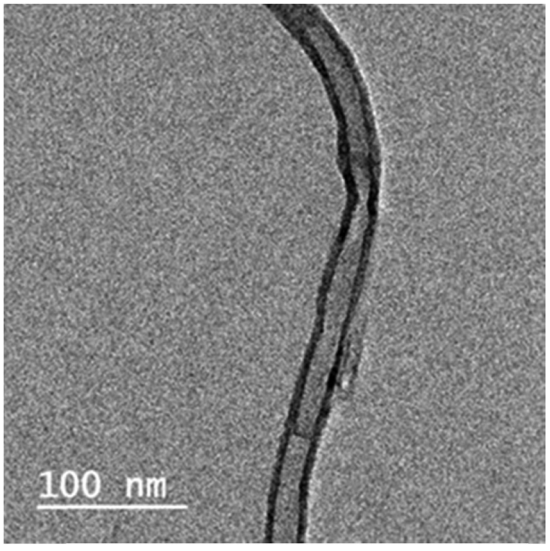

Figure 5: TEM image of CNTs [77]. Copyright: 5943171182537.

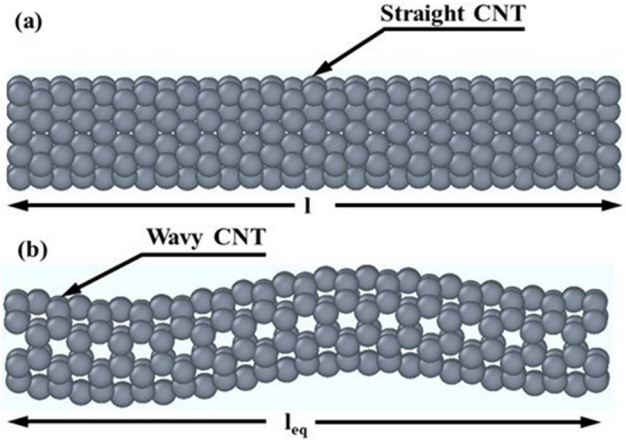

Figure 6: (a) Straight CNT and (b) wavy CNT.

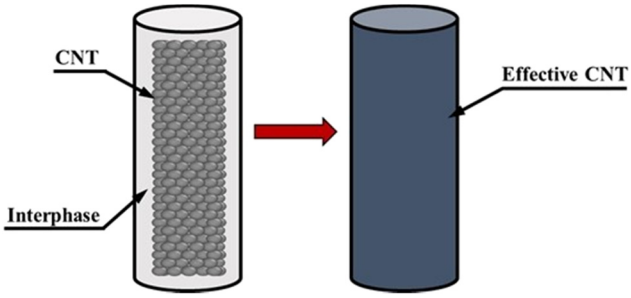

Figure 7: Effective CNT with interphase.

$$\phi_{\text{eff}} = \frac{(R + t)^2(\frac{l}{u} + 2t)}{\frac{R^2 l}{u}}\phi_{\text{f}}. \tag{31}$$

However, it is found that several CNTs are employed within the continuous network after percolation, while others are dispersed in CNT-polymer nanocomposites. Then, the percentages of a network of percolated CNTs are expressed as

$$f = \frac{(\phi_{\text{eff}})^{1/3} - (\phi_{\text{p}})^{1/3}}{1 - (\phi_{\text{p}})^{1/3}}. \tag{32}$$

The proposed equation for ϕ_{eff}, f, and σ_{N} can be assumed in Eq. (21) in order to predict the EC of CNT-polymer nanocomposites based on the tunneling mechanism. The mechanism is implemented by considering CNTs interphase, waviness of CNTs, and aspect ratio of CNTs.

2.1.2 Simulation of EMI SE

In order to estimate the EMI SE, a theoretical model was derived by Sevgi [2]. In this model, a conductive shielding plate of infinite extent is inserted between the EM-rays emitted device and the EM-rays absorbed device. This configuration is made in order to estimate the SE. It is noted that the SE of a material is a cumulative effect of absorption, reflection, and multiple internal reflections. However, absorption is a major shielding mechanism, and reflection is a secondary shielding mechanism, as shown in Figure 8. Further, multiple internal reflections are neglected when the SE due to absorption is ≥10 dB.

SE due to absorption (SE_{A}) loss is given by

$$\text{SE}_{\text{A}} = 20\log_{10}\left[\exp\left(\frac{\text{b}}{\delta}\right)\right], \tag{33}$$

where b and δ denote the thickness of shielding material and skin depth, respectively. The skin depth is defined as that distance below the surface of a conductor where the current density has diminished to $1/e$ of its value at the surface. The skin depth is expressed as

$$\delta = \sqrt{\frac{2}{\omega\sigma\mu}}, \tag{34}$$

where ω is the angular frequency of incident EM waves ($\omega = 2\pi n$), n is the frequency of EM waves in Hz, and μ is the magnetic permeability ($\mu = \mu_{\text{o}}\mu_{\text{r}}$, where $\mu_{\text{o}} = 4\pi \times 10^{-7}\text{H/m}\mu$ and μ_{r} is the relative permeability). By considering this, the above equation can be rewritten as

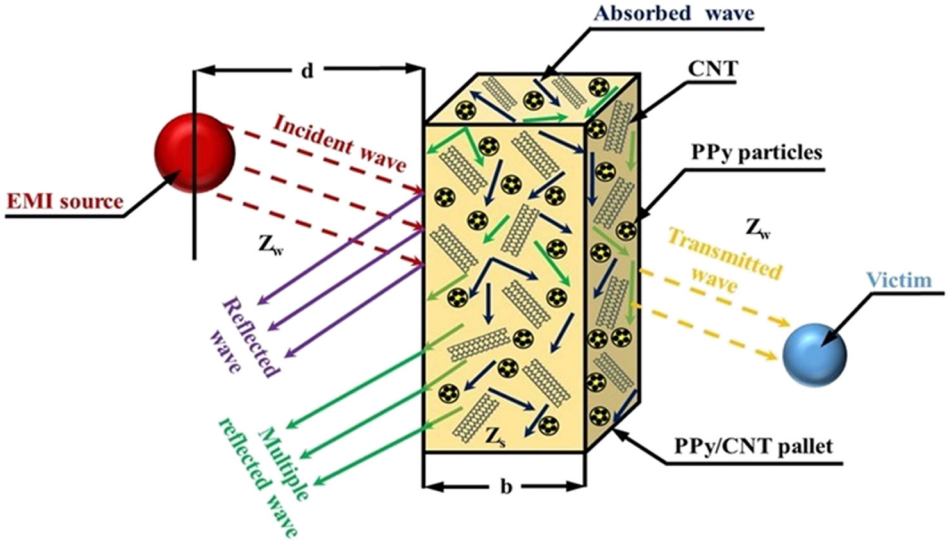

Figure 8: EM shielding material with the demonstration of absorption, reflection, and multiple reflection losses.

$$\delta = \frac{0.066}{\sqrt{n\sigma_r\mu_r}}. \tag{35}$$

Changing Eq. (35) into Eq. (33), the SE due to absorption can be obtained as

$$SE_A = 131.4b\sqrt{n\sigma_r\mu_r}, \tag{36}$$

where σ_r is the relative conductivity of CNT-polymer nanocomposites, with respect to copper in S/m (given as $\sigma_r = \sigma/\sigma_{Cu}$, $\sigma_{Cu} = 5.87 \times 10^7$ S/m).

The SE due to reflection (SE_R) can be obtained by considering the wave impedance (Z_w) and the conductor impedance (Z_s). This is expressed as follows:

$$SE_R = 20\log_{10}\left(\frac{E_i}{E_t}\right) = 20\log_{10}\left[\frac{(Z_s + Z_w)^2}{4 \quad Z_sZ_w}\right], \tag{37}$$

where E_i and E_t denote the strength of the incident electric field (EF) and the transmitted EF, respectively. It is to be noted that the impedance of shielding material can be expressed as

$$Z_s = \sqrt{\frac{\omega\mu}{\sigma}}. \tag{38}$$

Also, for the far field, the (plane) wave impedance in free space can be written as

$$Z_w = Z_o = 120\pi. \tag{39}$$

By converting Eqs. (37) and (38) into Eq. (36), the SE due to reflection can be reduced as follows:

$$SE_R = 20\log_{10}\left[\frac{1}{4}\sqrt{\frac{\sigma_r}{\mu_r n}}\right] = 168 + 10\log_{10}\left[\frac{\mu_r}{\mu_r n}\right]. \tag{40}$$

However, it is to be noted that, in the near field, the type of interfering source becomes one of the important factors. The wave impedance of electrical (*i.e.*, dipole-like emitting) sources is $Z_{we} = Z_o(2\pi d/\lambda)$, while the wave impedance of magnetic sources is $Z_{wm} = Z_o(2\pi d/\lambda)\Omega$. Therefore, the SE due to reflection for magnetic source and electric source can be expressed as

$$SE_{Rm} = 14.6 + 10\log_{10}\left[\frac{nd^2\sigma_r}{\mu_r}\right], \tag{41}$$

$$SE_{Re} = 332 + 10\log_{10}\left[\frac{\sigma_r}{\mu_r n^3 d^2}\right]. \tag{42}$$

If $d \le \frac{\lambda}{2\pi}$, then Eqs. (40) and (41) can be used for the estimation of SE due to reflection. For all other cases, Eq. (39) can be used for the estimation of SE due to reflection. Finally, the total SE is the sum of the contributions from SE due to absorption and reflection. It can be expressed as

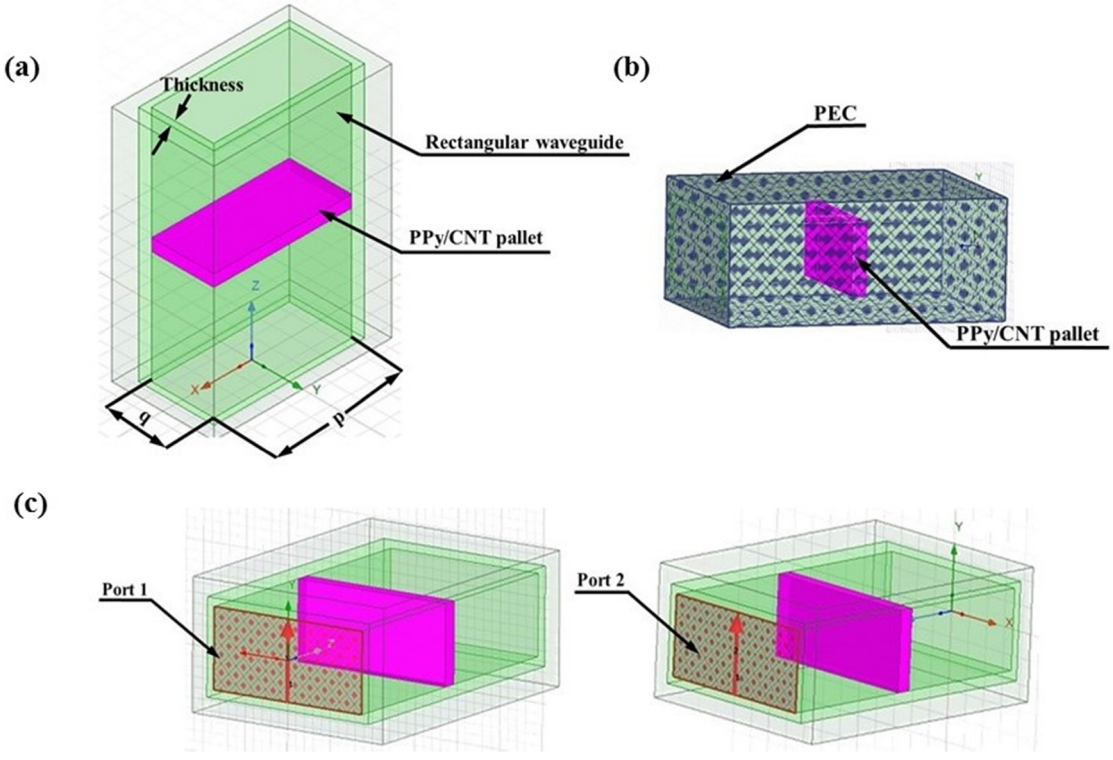

Figure 9: A rectangular waveguide with (a) loaded CNRC, (b) PEC boundary condition, and (c) two ports.

$$SE_T = SE_A + SE_R. \quad (43)$$

2.2 FE modeling

In this section, an FE model is developed using the commercially available software Ansys HFSS (high-frequency structure simulator). The EMI SE of CNRC in the C-band is estimated using this model. In this model, first, a rectangular waveguide (WR-137) with a standard dimension and cut-off frequency is designed in the C-band region, as shown in Figure 9(a). The cut-off frequency is the frequency at which no propagation of the signal takes place through the waveguide. The cut-off frequency is expressed as follows:

$$f_c = \frac{c}{2}\sqrt{\left(\frac{y}{p}\right)^2 + \left(\frac{z}{q}\right)^2}, \quad (44)$$

where f_c denotes the cut-off frequency, p and q denote the width and thickness of the waveguide, c denotes the speed of light, and y and z denote the mode of propagation of the wave. In a rectangular waveguide, transverse EM mode cannot be propagated. However, either transverse electric (TE) or transverse magnetic mode can be propagated. Although the waveguide can support several modes of wave propagation, in the present analysis, we consider the dominant mode for the rectangular waveguide. This is because the dominant mode is the one that has the lowest cut-off frequency. Table 1 summarizes the dimension of a waveguide, with the cut-off frequency in the C-band. For a rectangular waveguide, the dominant mode is the TE10 mode with $y = 1$ and $z = 0$. Thus, Eq. (44) can be modified as

$$f_c = \frac{c}{2p}. \quad (45)$$

In order to simulate EMI SE in the Ansys HFSS, we put the CNRC in the middle of the waveguide, as shown in Figure 9(a). Next, we assign the perfect electric boundary condition (PEC) to the rectangular waveguide, as shown in Figure 9(c). In order to generate the EM radiation, two ports are created: one port is at the left side of the waveguide, while another port is set at the right side of the waveguide, as shown in Figure 9(c). Finally, the solution setup, frequency, and sweep setup are completed, and the simulation is run.

Table 1: The dimension of a waveguide with the cut-off frequency in the C-band

P (mm)	*q* (mm)	Thickness (mm)	f_c (GHz)
34.848	15.79	1.625	4.3

3 Results and discussion

This section presents the analytical outcomes for the tunneling conductivity of CNRC. For the recognition of the tunneling effect, we have considered the aspect ratio, waviness, and interphase thickness of CNTs. Subsequently, we have reported the analytical outcomes of the EMI SE of CNRC as a function of the concentration of CNTs and the thickness of CNRC in the C-band (4.2–8.2 GHz). An FE model is also developed in order to estimate the EMI SE in the C-band region. A comparative report of the analytical and the numerical results is presented herewith.

3.1 Effect of tunneling conductivity of CNTs on CNRC

In order to determine the effect of the aspect ratio of CNTs on the EC of CNRC, the PPy and the CNTs are used as the matrix and reinforcement material, respectively. We mixed the CNTs in a PPy at different wt%, in order to improve the EC of CNRC. The aspect ratio of CNT is defined as the length-to-diameter ratio of CNT. In the present investigation, we varied the length of CNT while keeping its diameter constant. The EC of CNT and PPy are taken as

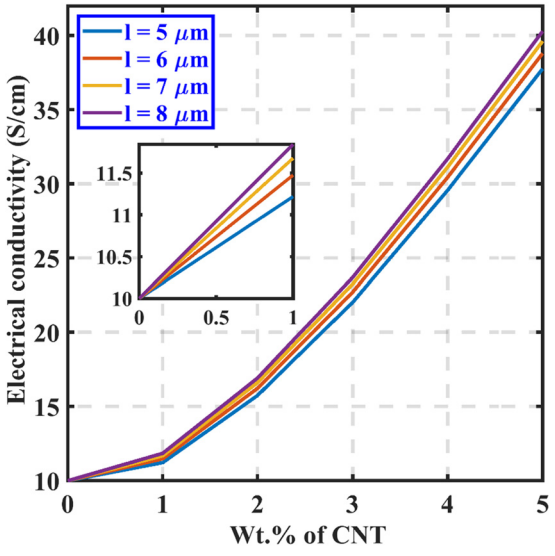

Figure 10: The EC of CNRC at different wt% and aspect ratio of CNTs (R = 15 nm, u = 1.43, t = 2.5 nm, and s = 8 nm).

10^6 S/m [79] and 10 S/cm [80], respectively. Figure 10 illustrates the variation of the EC of CNRC with respect to the concentration of CNTs. It is estimated that the EC of CNRC is improved by the incorporation of CNTs into the PPy matrix. Moreover, the EC of CNRC with long CNTs is higher compared to the EC of CNRC with short CNTs. This is attributed to the fact that EC is directly proportional to the length of CNTs. The EC of CNTs is much higher compared to the EC of PPy. Therefore, a remarkable improvement in the EC is obtained when CNTs are dispersed in PPy. This is attributed to the percolation conductive network of CNTs formed in the PPy matrix. It is observed that the EC path does not get established between the CNTs when the short CNTs are dispersed in a lower amount into the PPy matrix due to the large gap. Electrons flow among CNTs *via* the PPy matrix. However, by increasing the aspect ratio and concentration of CNTs, a dense and strong conductive network is established among CNTs in the PPy matrix. Due to this, more contact joints are formed among CNTs, which allow more electrons to be carried over a longer distance. Based on Figure 10, it may be concluded that the EC of CNRC improves through the incorporation of long CNTs in a higher quantity. It may be noted that earlier researchers have reported similar outcomes in predicting EC [61,78].

Figure 11 demonstrates the EC with respect to the wt% of CNTs at different interphase thicknesses. The interphase thickness is defined as the thickness of the interphase zone formed between the CNTs and PPy matrix. The figure depicts that the EC of the CNRC increases significantly, with an increase in the amount of CNTs within the PPy matrix. Also, it is notable that the EC of CNRC with a thick interphase is higher when compared to the EC of CNRC with a thin interphase. This reveals that a high tunneling conductivity is obtained by using a thick interphase and a high concentration of CNTs. The interphase thickness can be changed by altering the tunneling distance. A thick interphase thickness has been obtained at a low tunneling distance. The interphase creates a layer around nanotubes, which approaches the nanotubes and produces a conductive network. A thicker interphase region produces better interphase conductivity and a smaller interphase resistance in nanocomposites. Due to this, a dense conductive network is established in a CNRC. A dense conductive network allows the transmission of more electrons. Therefore, the EC of the nanocomposite shows a direct dependency on the interphase thickness. It can be concluded that interphase thickness also plays a positive role in percolation threshold, effective CNT, and the percentage of network CNT. The beneficial effect of interphase thickness on the EC of CNRC is reported in previous studies [60,78]. Therefore, it can be observed that increased interphase thickness reflects a positive change in the EC.

In order to investigate the effect of the waviness of CNTs on the EC of CNRC, we vary the equivalent length of the CNTs. Figure 12 illustrates the EC of CNRC for wavy and straight CNTs at different wt% of CNTs. It is found that the EC of CNRC is enhanced due to the incorporation of CNTs in the PPy matrix. However, the EC of CNRC with straight CNTs is greater compared to the EC of CNRC with wavy CNTs for the same loading of CNTs. It can be noticed that a low waviness factor significantly improves the

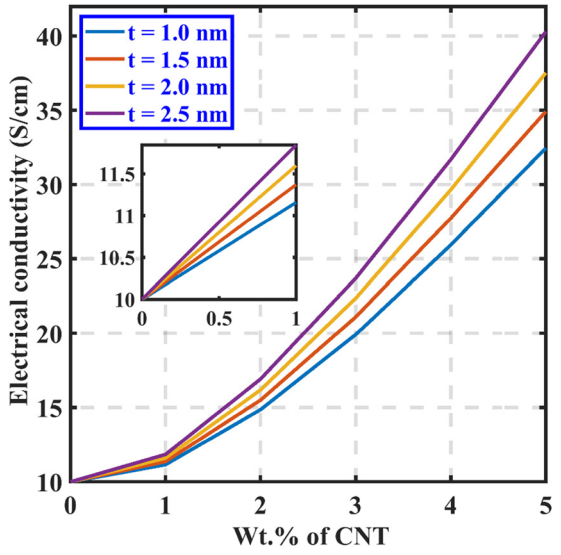

Figure 11: The EC of CNRC at different wt% of CNTs and interphase thickness (R = 15 nm, u = 1.43, l = 8 μm, and s = 8 nm).

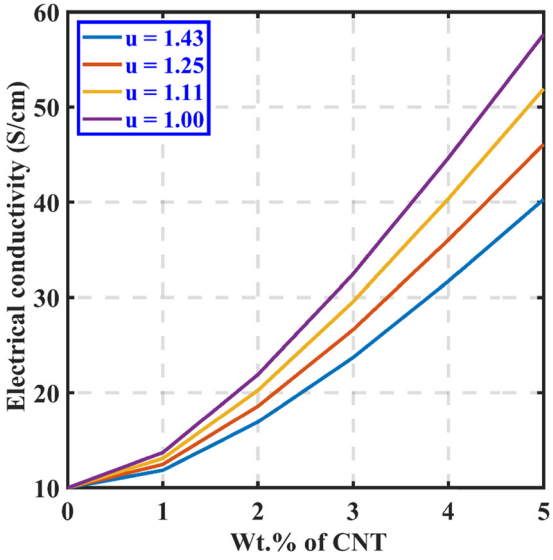

Figure 12: The EC of CNRC at different wt% of CNTs and different waviness factor (R = 15 nm, t = 2.5 nm, l = 8 μm, and s = 8 nm).

effectiveness of the EC of CNRC. Whereas the high waviness factor of CNTs depicts the higher curvature which degrades the effectiveness of the EC of CNRC. The increase in waviness of CNTs reduces the effective length of CNT. Subsequently, a weak conductive network is established between the CNTs in the PPy matrix. Thus, the electrons cannot be moved longer since the electrons are trapped in the PPy matrix. This provides a poor EC of CNRC containing wavy CNTs compared to straight CNTs. The detrimental effect of the curvature of CNTs on the EC of CNT-polymer nanocomposites is also reported in previous studies [81,82]. So, it can be concluded that the straight CNTs produce low percolation thresholds and high effective filler concentrations. As a result, straight CNTs produce larger networks in nanocomposites.

3.2 EMI SE of CNRC

In order to study the performance of CNRC in EMI SE, analytical outcomes are estimated based on the model derived in the previous section. The total SE is defined as the ability of a material to attenuate the incident EM radiation. For this, Eq. (42) is formulated, and the tunneling conductivity of CNRC is estimated. In order to verify the validity of the analytical model derived in Section 2, we compare the total SE (SE_T) at a frequency of 8.2 GHz, as per the findings of Gahlout and Choudhary [33] and those relating to Ansys HFSS. Figure 13 illustrates the variations of the SE_T analytically, numerically, and theoretically, at different wt% of the CNTs. It can be observed that the

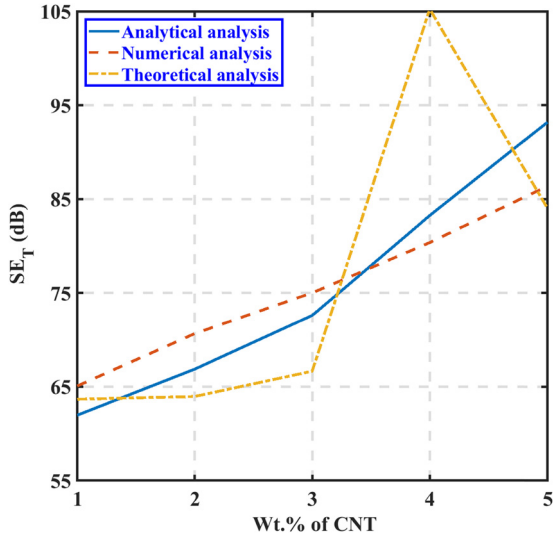

Figure 13: Variations of the total EMI SE of CNRC at different wt% of the CNT and at a frequency of 8.2 GHz.

Ansys HFSS outcomes overestimate the value of SE_T up to 3wt% loading of CNTs. Whereas the outcomes of theoretical analysis show better agreement with the analytical results, except at 4 wt%. Such discrepancy exists because the tunneling conductivity of CNTs is considered while estimating the analytical outcomes. Figure 13 shows good agreement among the present model, the existing study, and the Ansys HFSS outcomes. Hence, the validity of the proposed model is verified.

To further understand the shielding process of CNRC, we utilized HFSS simulation to analyze the magnetic field (MF) and EF distributions of CNRC while blocking EM waves, as shown in Figure 14(a)–(h). In order to make things easier, R1 and R2, which correspond to VNA ports 1 and 2, are configured to generate EF and MF excitation and receive EM signals, respectively. Figure 14(a) and (b) depict how the EF and MF are distributed in the unloaded waveguide. The generated EM waves from excitation source R1 are readily received by R2 due to the lack of a barrier and significant EF and MF distributions. However, when the conductive pallet at 1% loading of CNT is placed in the middle of the waveguide, the produced EM waves from the excitation source R1 may penetrate to this pallet and be received by R2, as seen in Figure 14(c) and (d). This low level of EM wave penetration implies that this pallet has high EM wave attenuation and shielding capacity (~66 dB attenuation of EM waves, 99.99% attenuation of EM waves). Increasing the MWCNT loading to 3% results in a considerable reduction in the strength of EF and MF in R2, as seen in Figure 14(e) and (f).

This illustrates outstanding shielding capabilities of the pallet at 3% loading of CNT. The EF and MF distributions in R2 disappear entirely when the MWCNT loading is increased to 5%, as illustrated in Figure 14(g) and (h). The MF component of the EM wave in a waveguide is very low, as illustrated in Figure 14(b), (d), (f), and (h), showing that there is very little magnetic loss in the interaction between the nanocomposites and the EM wave. As a result, conductive loss, which includes reflection and absorption, accounts for the bulk of EM wave attenuation, which agrees with experimental data.

Figure 15 illustrates the variations in SE due to absorption (SE_A) and reflection (SE_R), within the frequency range of 4.2–8.2 GHz, at different wt% of CNTs. The figure depicts that the SE_A is enhanced as the concentration of CNTs in the PPy matrix increases. This increasing trend is maintained throughout the C-band region, as shown in Figure 15(a). Whereas the SE_R increases as the wt% of CNTs in the PPy matrix increases. However, for the higher frequency range in the C-band, the effective value of SE_R decreases, as shown in Figure 15(b). It is noted that as the concentration

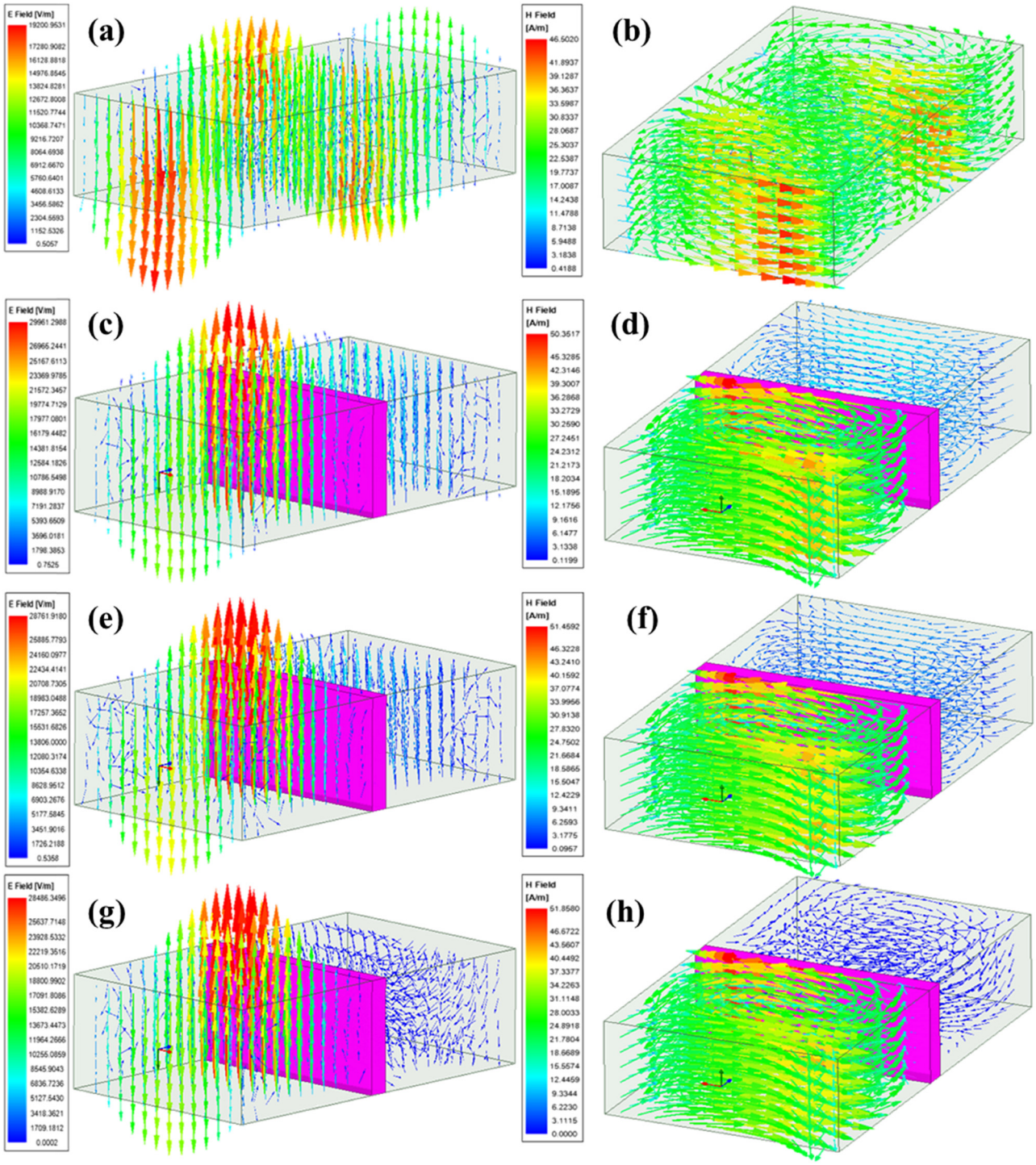

Figure 14: Electric and MF intensity distribution in WR-137 waveguide at a frequency of 8.2 GHz: (a) and (b) no sample loading, (c) and (d) 1% loading of CNT, (e) and (f) 3% loading of CNT, and (g) and (h) 5% loading of CNT.

of CNTs increases, the formation of electric and magnetic dipoles also increases in the CNRC. The enhanced electric dipole increases the pair of opposite charges in the CNRC. Subsequently, it increases the dielectric constant of the CNRC. However, the enhanced magnetic dipole increases the pair of poles in the CNRC. Subsequently, it increases the magnetic permeability of the CNRC. Therefore, a material with a high dielectric constant and magnetic permeability absorbs more EM radiation. In addition, the increased concentration of CNTs in the PPy matrix entails the existence

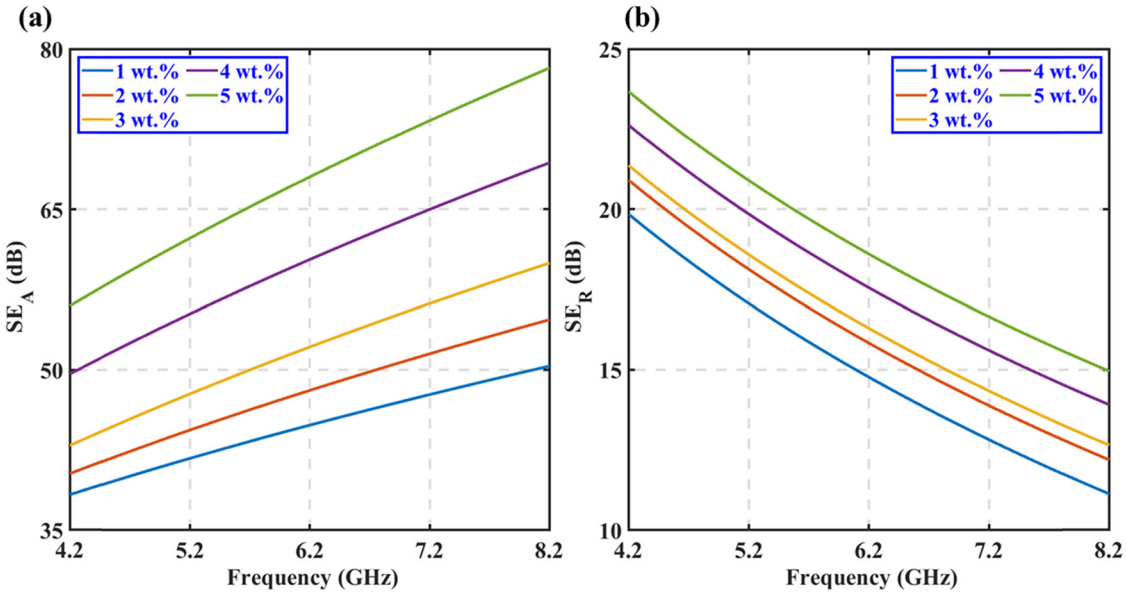

Figure 15: EMI SE of CNRC at different wt% of CNT due to (a) absorption (SE_A) and (b) reflection (SE_R) (R=15 nm, u = 1.43, l = 8 μm, s = 8 nm, t = 2.5 nm, d = 30 cm, and b = 3 mm).

of more mobile charge carriers, such as electrons or holes, which make the material more conductive. The EM waves get reflected when they come into contact with the highly conductive material. Figure 16 depicts the variations of the SE_T of CNRC, in the C-band region, at various wt% of CNTs. The figure shows that the SE_T, which is the contribution made by SE through absorption and reflection, is enhanced by the incorporation of CNTs in the PPy matrix. Therefore, it can be concluded that the incorporation of CNTs in the PPy matrix improves the SE_T. It may be noted that the previous studies reported a similar effect on the EMI SE of CNT-polymer nanocomposite following the incorporation of CNTs [83,84]. Table 2 shows the values of the SE of CNRC at different wt% of CNTs and at a frequency of 8.2 GHz.

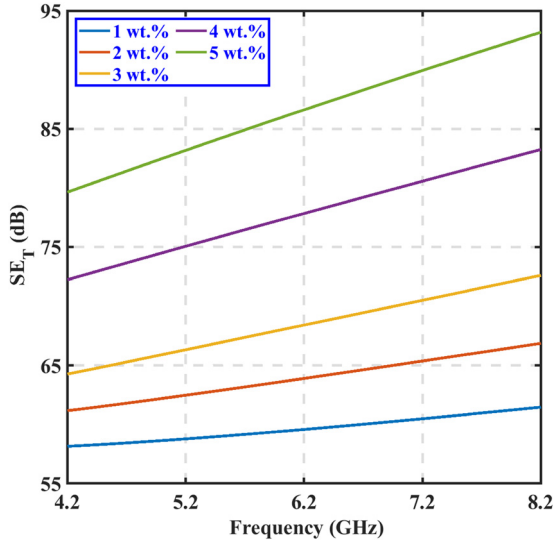

Figure 16: Total EMI SE of CNRC at different wt% of CNT (R = 15 nm, u = 1.43, l = 8 μm, s = 8 nm, t = 2.5 nm, d = 30 cm, and b = 3 mm).

In order to estimate the effect of the thickness of CNRC on EMI SE, we modeled the CNRC at different levels of thickness and at a constant 3 wt% of CNTs. Figure 17 demonstrates the EMI SE properties at different thickness levels of CNRC in the C-band region. Figure 17(a) depicts that SE_A is enhanced with increased thickness of CNRC, and such an incremental trend is maintained in the C-band region. However, the thickness of CNRC nanocomposites does not impact the SE_R. It can be observed that the SE_R decreases even if the frequency of the C-band increases. Also, the layers of conductive mesh increase with the thickness of CNRC. These conductive layers are randomly established in the CNRC, one after another. Subsequently, increasing the number of layers of conductive mesh increases the absorption of EM waves, as shown in Figure 18. Our analytical formulation

Table 2: The SE of CNRC at different wt% and at a frequency of 8.2 GHz

wt% of CNTs	SE_A (dB)	SE_R (dB)	SE_T (dB)
1	50.34	11.12	61.46
2	54.68	12.18	66.86
3	59.95	12.64	72.60
4	69.33	13.90	83.24
5	78.22	14.90	93.17

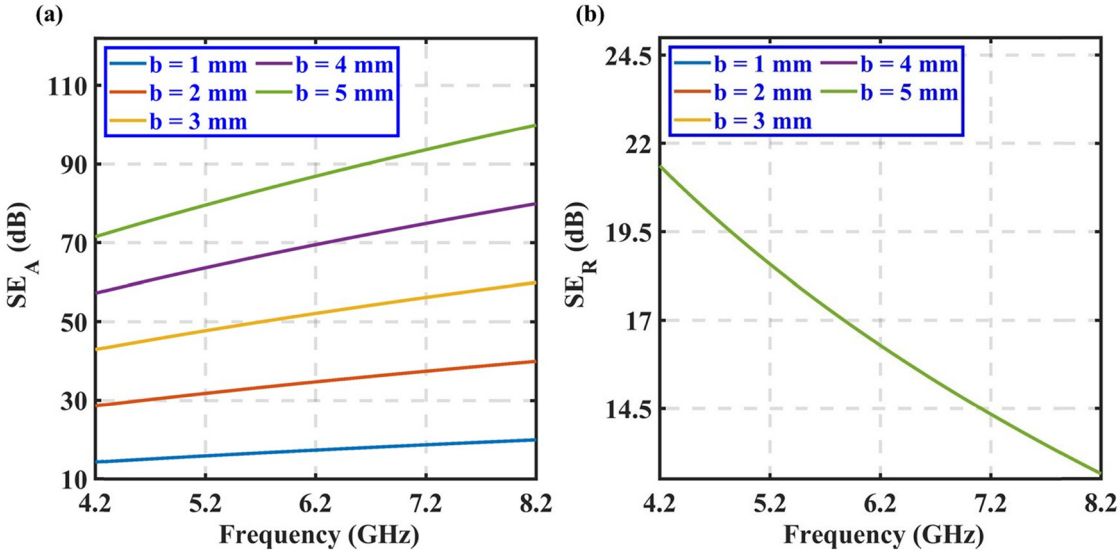

Figure 17: EMI SE of CNRC at various thickness levels of nanocomposites due to (a) absorption (SE_A) and (b) reflection (SE_R) (R = 15 nm, u = 1.43, l = 8 μm, s = 8 nm, t = 2.5 nm, d = 30 cm at 3 wt% of CNT).

shows the direct dependency of SE_A on nanocomposite thickness. According to EM theory, SE due to reflection is not a function of the thickness of the nanocomposite. Moreover, it is also found that the EC is not a function of the thickness of the CNRC. Thus, when the EM wave strikes the CNRC, it reflects the same amount of radiation, as shown in Figure 17(b). The SE_T of CNRC is illustrated in Figure 19. The figure shows that SE_T increases as the sample thickness in the C-band region increases. Similar outcomes were also reported by previous studies. Thus, it can be concluded that the EMI SE increases with the thickness of nanocomposite [85,86]. Table 3 shows the values of SE of CNRC at different thickness levels of CNRC and a frequency of 8.2 GHz.

In order to investigate the effect of tunneling conductivity of CNTs on the EMI SE of a CNRC, we vary the equivalent length, interphase thickness, and waviness of the CNTs. This analysis is carried out at a constant 3 wt% of CNTs in the PPy matrix. Figure 20 demonstrates SE_T at different tunneling conductivities of the CNTs. It can be observed that SE_T increases with the length of a CNT, and this incremental trend is maintained in the frequency range of 4.2–8.2 GHz, as shown in Figure 20(a). The SE_T at various interphase thicknesses is illustrated in Figure 20(b). From Figure 20(b), it can be observed that as the interphase thickness increases, the total shielding effectiveness SE_T also increases. This is attributed to the fact

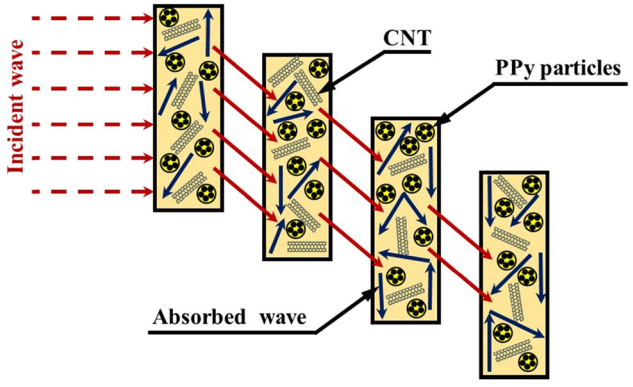

Figure 18: Mechanism of EMI absorption by different layers of CNRC.

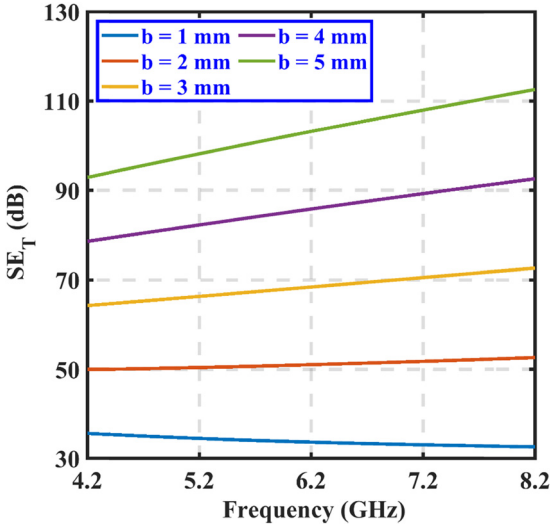

Figure 19: Total EMI SE of CNRC at various thickness levels of nanocomposites (R = 15 nm, u = 1.43, l = 8 μm, s = 8 nm, t = 2.5 nm, d = 30 cm at 3 wt% of CNT).

Table 3: The SE of CNRC, at various thickness levels of CNRC, and at a frequency of 8.2 GHz

Thickness of CNRC (mm)	SE_A (dB)	SE_R (dB)	SE_T (dB)
1	19.98	12.64	32.63
2	39.96	12.64	52.61
3	59.95	12.64	72.60
4	79.93	12.64	92.58
5	99.92	12.64	112.57

that increasing the length and interphase thickness of CNTs increases the contact joints between CNTs. Therefore, a dense and strong conductive network is established between CNTs. This increases the EC of CNRC, as discussed in the previous section. Subsequently, when EM radiation interacts with this conductive material, it increases the SE_T. However, Figure 20(c) shows the variations of SE_T at various waviness levels of CNTs. It may be seen from Figure 20(c) that the SE_T decreases as the waviness of CNTs increases. It is found that the effective length of CNT decreases due to its waviness. Thus, a weak conductive network is established between the CNTs in the PPy matrix. This weak conductive network reduces the EC of CNRC. Therefore, SE_T of the CNRC also decreases with the increase in the waviness of CNTs. Based on this, we can conclude that SE_T increases with the length, interphase thickness, and straightness of CNTs.

Table 4 shows the overviews of the EMI SE of different polymer nanocomposites reported by previous research and

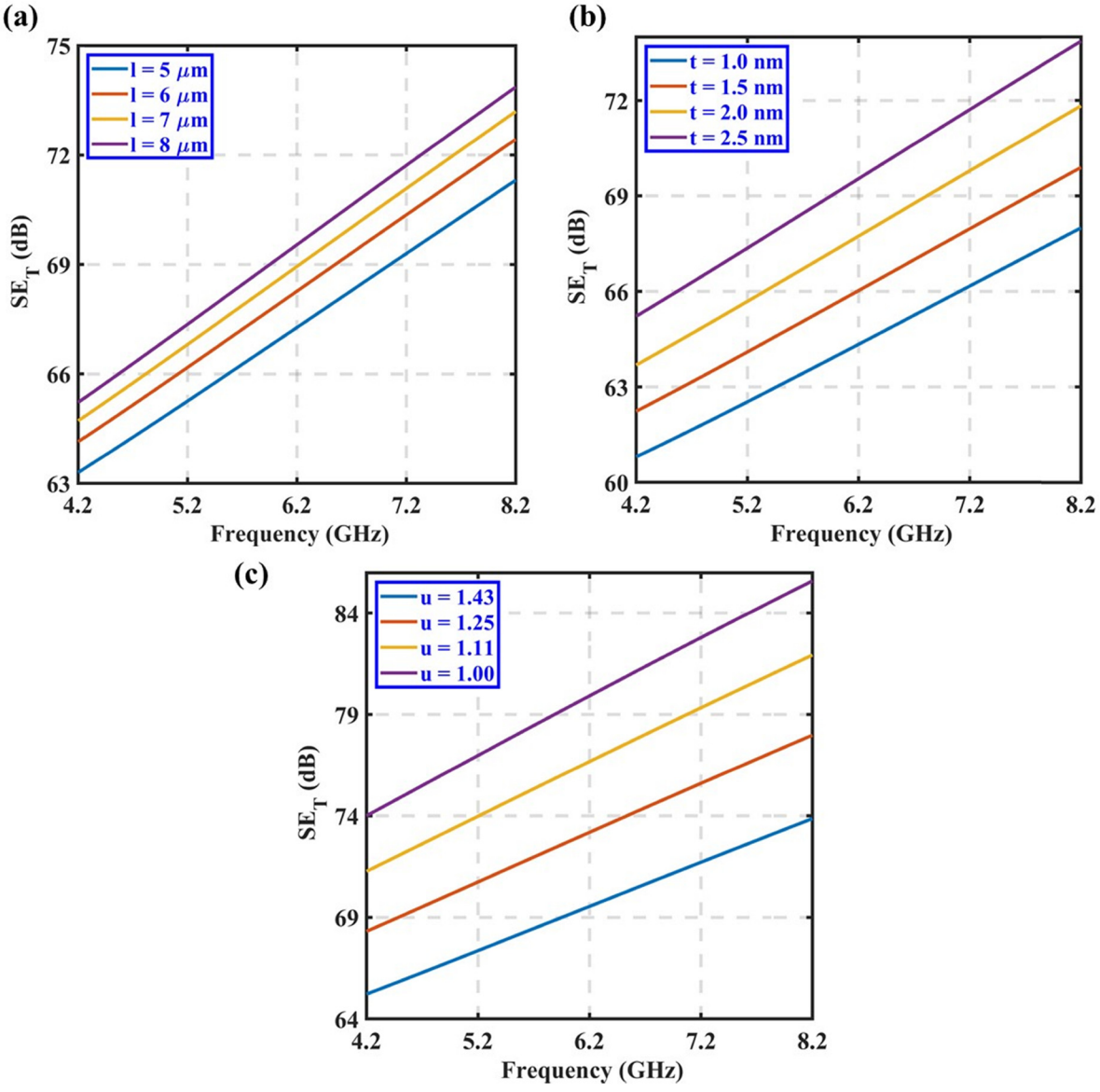

Figure 20: Total EMI SE of CNRC at various (a) length of CNTs, (b) interphase thickness, and (c) waviness of CNTs (R = 15 nm, s = 8 nm, d = 30 cm at 3 wt% of CNT).

Table 4: Overview of EMI SE of different polymer nanocomposites

Nanocomposite	Thickness (mm)	Frequency (GHz)	Shielding performance (dB)	References
MWCNT/polyethylene	1	8.2	50	[87]
MWCNT/epoxy	2	18	68	[88]
MWCNT/PPy	3	8.2	120.89	[33]
MWCNT/polycaprolactone	30	35	45	[89]
MWCNT/polycaprolactone	2	12	80	[90]
MWCNT/polylactic acid	0.4	12	55	[91]
MWCNT/PPy	3	8.2	93.17	Present study

the current study. This table shows that the EMI SE of the newly developed nanocomposite is comparable to that of the pallets. Figure 21 demonstrates the EC enhancement factor (ECEF) with respect to wt% of CNTs. The ECEF shows the percentage enhancement of the EC of CNRC, as compared to the base nanocomposite and given by

$$\text{ECEF} = \frac{\text{EC}_{\text{CNT}} - \text{EC}_0}{\text{EC}_0} \times 100, \tag{46}$$

where EC_{CNT} denotes the EC of CNRC, and EC_0 represents the EC of the base nanocomposite material. In order to estimate the ECEF at different aspect ratios, interphase thicknesses, and waviness levels, we assume that the base

3.3 Quantitative relative analysis of CNRC

In this section, we present the quantitative analysis of CNRC for the various wt% of CNTs at different aspect ratios, interphase thicknesses, and waviness levels. Quantitative analysis is important for selecting the optimum range of these parameters in order to achieve the maximum EC of

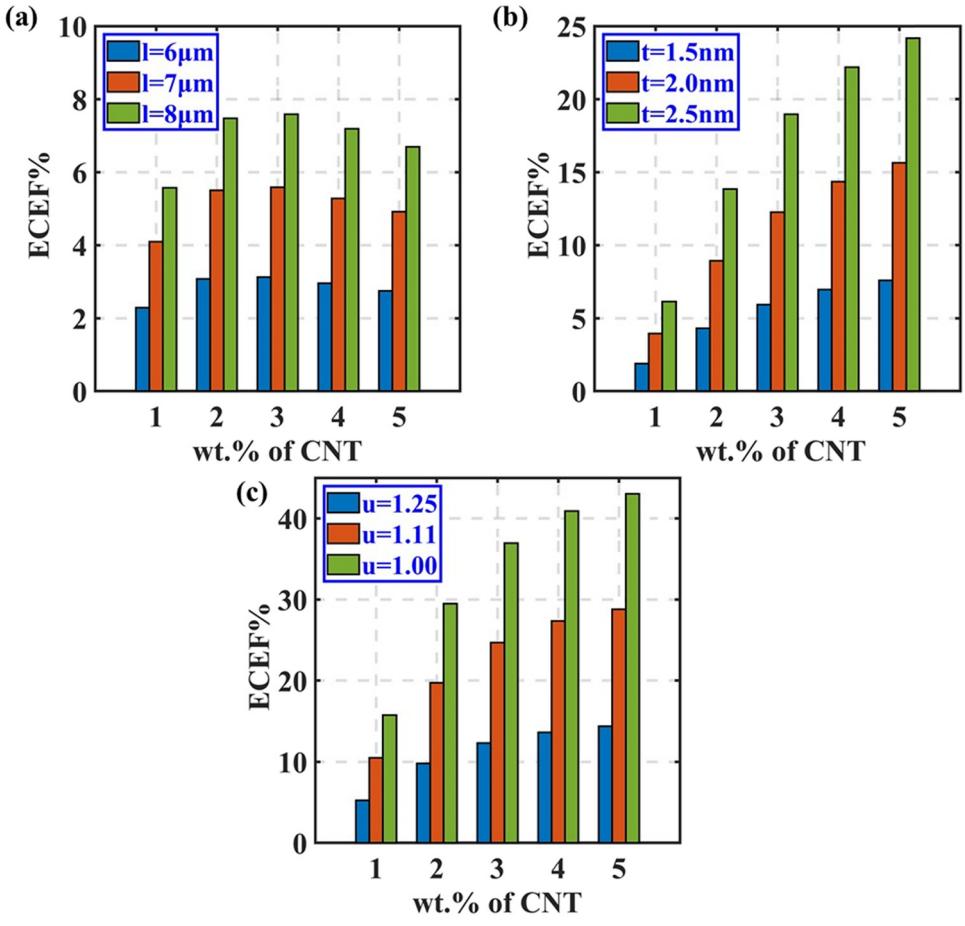

Figure 21: Variation of ECEF with different amounts of CNTs at varying (a) length of CNTs, (b) interphase thickness, and (c) waviness of CNTs.

composite has CNTs with length = 5 μm, interphase thickness = 1 nm, and waviness factor = 1.43.

Figure 21(a) illustrates the variations in ECEF, with the wt% of CNT, at various aspect ratios, by varying the length and keeping the diameter of the CNTs constant. It can be observed that the value of ECEF increases as the wt% of CNT increases in the CNRC. Here, the maximum value of ECEF is observed at 3 wt%. We also observed that the value of ECEF increases as we increase the aspect ratio by varying the length of CNTs from 6 to 8 μm. At 3 wt%, the maximum values of ECEF are 3.4, 5.8, and 7.59% corresponding to the values of length 6, 7, and 8 μm, respectively. The influence of interface thickness on ECEF is shown in Figure 21(b). This figure depicts that the ECEF increases as the interface thickness and the wt% of CNTs increase. The maximum value of ECEF is 24.16%, corresponding to t = 2.5 nm and wt% of CNT = 5. This is attributed to the fact that the EC directly depends on the interphase thickness and wt% of CNTs. Figure 21(c) represents the influence of the waviness factor on the ECEF of CNRC at various wt% of CNTs. In this figure, we observe that the ECEF increases as the wt% of CNTs increases from 1 to 5. Also, it can be seen that ECEF reduces as the waviness factor increases. Thus, we can conclude that the waviness factor of the CNTs should be kept low in order to achieve a higher value of ECEF. In addition, from Figure 21(a)–(c), we can conclude that, to obtain a higher value of ECEF, the CNTs in the CNRC should be kept within the range of 3–5 wt%.

To demonstrate the enhancement in the EMI SE of the CNRC, an EMI shielding enhancement factor (ESEF) is defined. This ESEF shows the percentage improvement in EMI SE of CNRC. as compared to the base nanocomposite. Hence, ESEF can be given by:

$$\text{ESEF} = \frac{E_{\text{CNT}} - E_0}{E_0} \times 100, \tag{47}$$

where EC_{CNT} denotes the EMI SE of CNRC, and E_0 represents the EMI SE of the base nanocomposite. To estimate the ESEF at different wt% of CNTs and various thickness levels of CNRC, we assume that the base composite has 1 wt% of CNTs and thickness of 1 mm, respectively. However, to estimate the ESEF at different aspect ratios, interphase thickness, and waviness, we assume that the base composite has CNTs, with length = 5 μm, interphase thickness = 1 nm, and waviness factor = 1.43, respectively.

Figure 22 depicts the ESEF of a CNRC in the C-band region at various concentrations of the CNTs and thickness levels of a CNRC. From Figure 22(a), it can be observed that the value of ESEF increases as the wt% of CNT increases in the CNRC. Here, the maximum value of ESEF is observed at 5 wt%. We also found that the value of ESEF increases as the frequency increases from 4.2 to 8.2 GHz. At 5 wt%, the maximum value of ESEF is 79.30%, corresponding to the frequency of 8.2 GHz. This is due to the direct dependency of EMI SE of CNRC on wt% of CNRC. The influence of CNRC thickness on ESEF is demonstrated in Figure 22(b). This figure depicts that the ESEF increases as the thickness of the CNRC and the frequency increase. The maximum value of ESEF is reported as 245%, corresponding to b = 5 mm, at a frequency of 8.2 GHz. Thus, ESEF shows the direct dependency of EMI SE on the thickness of the nanocomposite. From this estimation, we can conclude that, to obtain a higher value of ESEF, the CNTs in the CNRC should be kept within the range of 3–5 wt% and the thickness of CNRC should be kept within the range of 3–5 mm.

Figure 23 illustrates the variations of ESEF of a CNRC in the C-band region at various lengths, interphase thickness levels, and waviness levels of CNTs. From Figure 23(a), it can be seen that the value of ESEF increases with an increase in the length of CNTs in the C-band. At a frequency

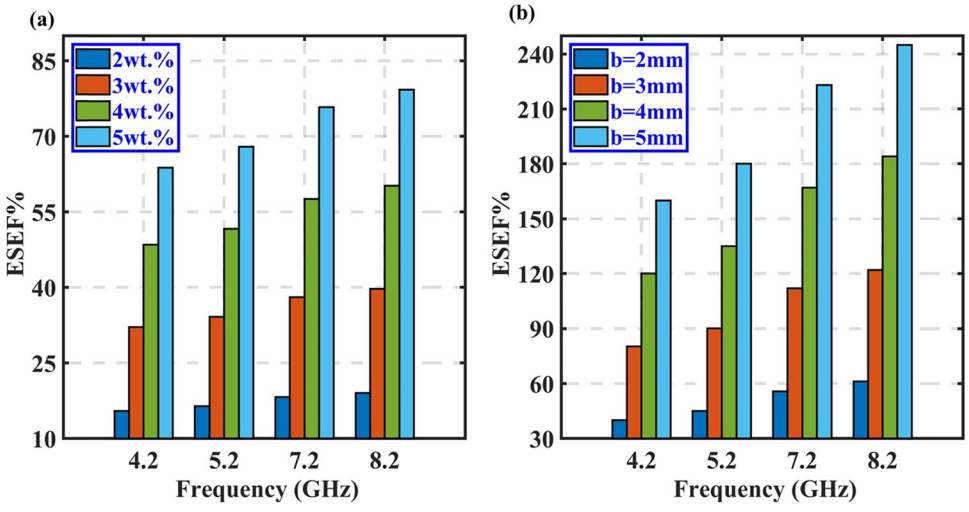

Figure 22: Variation of ESEF in the C-band region at different (a) amounts of CNT and (b) thickness levels of CNRC.

of 8.2 GHz, the maximum values of ESEF are 1.7, 2.8, and 3.58% corresponding to the values of length 6, 7, and 8 μm, respectively. The influence of interface thickness on ESEF is shown in Figure 23(b). This figure depicts that the ESEF increases as the interface thickness and the frequency increase. The maximum value of ESEF is 8.62%, corresponding to t = 2.5 nm, and a frequency of 8.2 GHz. However, the influence of the waviness factor on the ESEF of CNRC in the C-band is shown in Figure 23(c). In this figure, we observe that the ESEF increases as the frequency increases from 4.2 to 8.2 GHz. Also, it can be seen that ESEF falls as the waviness factor increases. At a frequency of 8.2 GHz, the maximum values of ESEF are 5.2, 11.1, and 15.55%, corresponding to the waviness factors of 1.25, 1.11, and 1, respectively. In addition, from Figure 23(a) to (c), we can conclude that, in order to obtain a higher value of ESEF, long CNTs with high interphase thickness and low waviness factor are to be preferred. Therefore, it can be concluded that the tunneling conductivity of CNTs affects the ESEF.

Figures 10–23 clearly show a significant enhancement in the EMI SE of the CNRC due to the inclusion of the tunneling conductivity of CNTs. The quantitative relative performance of CNRC can be determined by two factors: (i) ECEF for the change in EC and (ii) ESEF for the change in EMI SE of CNRC. This quantitative relative performance of CNRC is shown as a bar chart in Figures 21–23. On the basis of these results, one can estimate the EMI SE by varying different parameters such as aspect ratio, interphase thickness, waviness of CNTs, thickness of nanocomposite, and the wt% of CNTs. In addition, tunneling conductivity (aspect ratio, interphase thickness, and waviness of CNT) and EMI SE significantly contribute to advancements in material design for EM shielding applications. Based on the quantitative relative analysis, the results suggest that the maximum EMI SE of a CNRC can be obtained using long and straight CNTs as well as thick interphase at a high concentration level of CNTs. This allows to develop lightweight shielding materials that can replace heavy metallic shielding materials in a specific frequency range, which

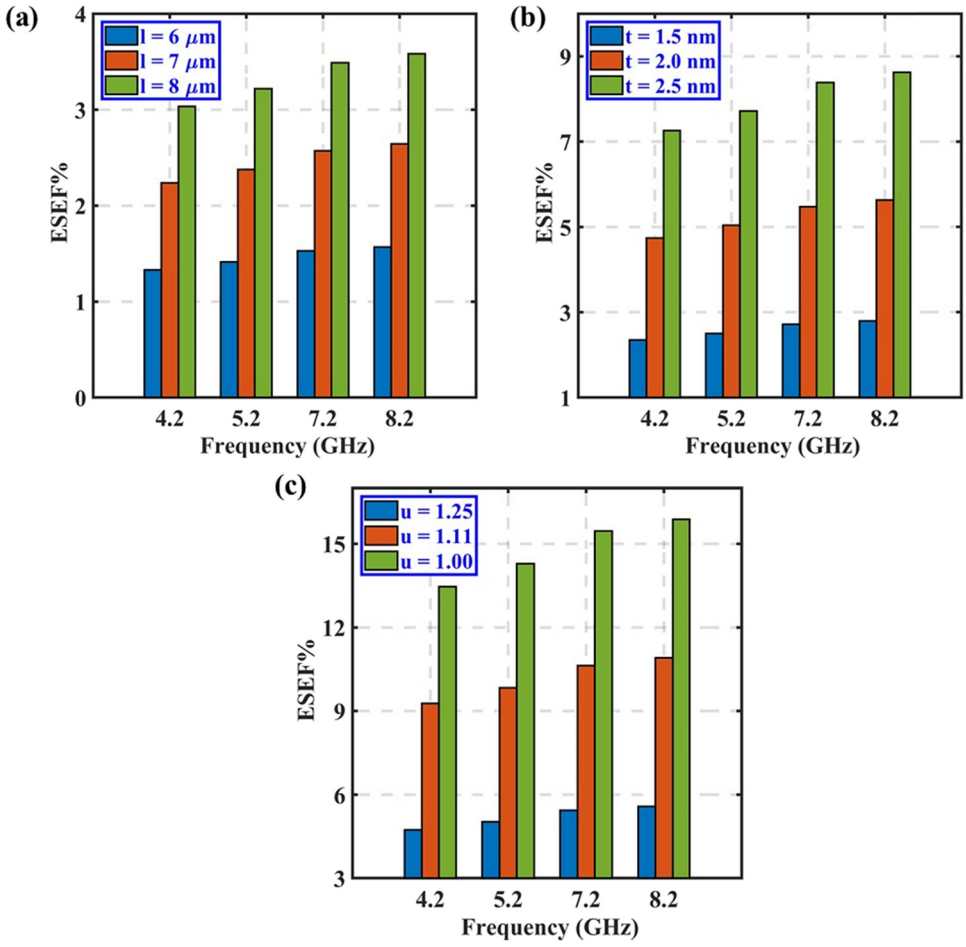

Figure 23: Variations of ESEF in the C-band region, at different (a) lengths of CNTs, (b) interphase thickness levels, and (c) waviness levels of CNTs.

depends on the required applications (*e.g.*, satellite communications, radar, 5G networks).

4 Conclusions

In the current study, an analytical model has been proposed to evaluate the EMI SE of CNRCs in the C-band (4.2–8.2 GHz) region, accounting for the tunneling conductivity of CNTs. First, we evaluated the EC of the CNRC by incorporating the CNTs at different wt% in the PPy matrix. This EC is evaluated by considering the tunneling conductivity of the CNTs. The tunneling conductivity of CNTs is estimated by varying the aspect ratio, interphase thickness, and waviness of the CNTs in the PPy matrix. Second, the EMI SE of CNRCs is predicted for varying CNT weight percentages, tunneling conductivity of CNTs, and the thickness of the CNRC. Our outcomes indicate a significant enhancement in the EC of the CNRC, resulting from the incorporation of CNTs into the PPy matrix. Also, it is found that the EC of a CNRC increases with an increase in the aspect ratio and interphase thickness of the CNTs. However, the EC decreases with an increase in the aspect ratio of the CNTs. This indicates a clear relationship between the EC of the CNRC and the tunneling conductivity of the CNTs. It may also be concluded that the EMI SE of a CNRC is enhanced greatly with an increase in the aspect ratio, interphase thickness, and wt% of CNTs. Nevertheless, the EMI SE of the CNRC decreases with an increase in the waviness of the CNTs. It is also noted that the EMI SE of the CNRC increases with an increase in the thickness of the nanocomposite. An FE model is also being developed to confirm the analytical findings and further understand the CNRC shielding process. Our numerical findings are in good agreement with the analytic findings. Based on the quantitative analysis, it may be concluded that the optimum EC and EMI SE of a CNRC are obtained by using long, thick interphase and straight CNTs, at a high concentration level of CNTs.

Acknowledgments: The authors would like to thank the Indian Space Research Organization (ISRO), the Government of India, and the Higher Education Financing Agency (HEFA, a joint venture of MoE-GOI and Canara Bank) for providing financial support. The corresponding author acknowledges the generous support of the RESPOND Program Grant of ISRO (ISRO/RES/3/813/19-20) and the Corporate Social Responsibility Scheme of HEFA (HEFA/CSR/IITI/01/2024-25) awarded to him.

Funding information: The authors would like to thank the Indian Space Research Organization (ISRO), the Government of India, and the Higher Education Financing Agency (HEFA, a joint venture of MoE-GOI and Canara Bank) for providing financial support.

Author contributions: Rajnish P. Modanwal: data curation, formal analysis, investigation, methodology, software, validation, visualization, writing – original draft. M. Gupta: formal analysis, investigation, validation, visualization, writing – review and editing. Shailesh I. Kundalwal: conceptualization, funding acquisition, investigation, methodology, project administration, resources, supervision, writing – review and editing. All authors have accepted responsibility for the entire content of this manuscript and approved its submission.

Conflict of interest: Authors state no conflict of interest.

Data availability statement: All data generated or analyzed during this study are included in this published article.

References

[1] Raina HS. Electromagnetic compliance in high power communication satellite payloads. IETE Tech Rev. 2005;22(4):273–85.
[2] Sevgi L. Electromagnetic screening and shielding-effectiveness (SE) modeling. IEEE Antennas Propag Mag. 2009;51(1):211–6.
[3] Xiang C, Pan Y, Guo J. Electromagnetic interference shielding effectiveness of multiwalled carbon nanotube reinforced fused silica composites. Ceram Int. 2007;33(7):1293–7.
[4] Saini P, Choudhary V, Singh BP, Mathur RB, Dhawan SK. Polyaniline–MWCNT nanocomposites for microwave absorption and EMI shielding. Mater Chem Phys. 2009;113(2–3):919–26.
[5] Beall C, Delzell E, Cole P, Brill I. Brain tumors among electronics industry workers. Epidemiology. 1996;7(2):125–30.
[6] Thomas TL, Stolley PD, Stemhagen A, Fontham ET, Bleecker ML, Stewart PA, et al. Brain tumor mortality risk among men with electrical and electronics jobs: a case-control study. J Natl Cancer Inst. 1987;79(2):233–8.
[7] Darraji M, Saqban L, Mutar T, Rasheed M, Hussein A. Association of candidate genes polymorphisms in Iraqi patients with chronic kidney disease. J Adv Biotechnol Exp Ther. 2022;6(1):687.
[8] Kherifi D, Keziz A, Rasheed M, Oueslati A. Thermal treatment effects on Algerian natural phosphate bioceramics: A comprehensive analysis. Ceram Int. 2024;50(17):30175–87.
[9] Gupta A, Choudhary V. Electromagnetic interference shielding behavior of poly (trimethylene terephthalate)/multi-walled carbon nanotube composites. Compos Sci Technol. 2011;71(13):1563–8.
[10] Al-Saleh MH, Sundararaj U. Electromagnetic interference shielding mechanisms of CNT/polymer composites. Carbon. 2009;47(7):1738–46.
[11] Chen YH, Huang ZH, Lu MM, Cao WQ, Yuan J, Zhang DQ, et al. 3D Fe_3O_4 nanocrystals decorating carbon nanotubes to tune

electromagnetic properties and enhance microwave absorption capacity. J Mater Chem A. 2015;3(24):12621–5.
[12] Lee SH, Kang D, Oh IK. Multilayered graphene-carbon nanotube-iron oxide three-dimensional heterostructure for flexible electromagnetic interference shielding film. Carbon. 2017;111:248–57.
[13] Kadri E, Dhahri K, Barille R, Rasheed M. Novel method for the determination of the optical conductivity and dielectric constant of SiGe thin films using Kato-Adachi dispersion model. Phase Transit. 2021;94(2):65–76.
[14] Saidi W, Hfaidh N, Rasheed M, Girtan M, Megriche A, Maaoui ME. Effect of B_2O_3 addition on optical and structural properties of TiO 2 as a new blocking layer for multiple dye sensitive solar cell application (DSSC). RSC Adv. 2016;6(73):68819–26.
[15] Modanwal RP, Murugesan J, Sathiaraj D. Tribological and Corrosion Behaviour of Non-Equiatomic Magnetic FeCoNiMnAl High Entropy Alloy. Tribol Int. 2024;198:109903.
[16] Kaur A, Dhawan SK. Tuning of EMI shielding properties of polypyrrole nanoparticles with surfactant concentration. Synth Met. 2012;162(15–16):1471–7.
[17] Vulpe S, Nastase F, Nastase C, Stamatin I. PAN–PAni nanocomposites obtained in thermocentrifugal fields. Thin Solid Films. 2006;495(1–2):113–7.
[18] Alshalal I, Al-Zuhairi HM, Abtan AA, Rasheed M, Asmail MK. Characterization of wear and fatigue behavior of aluminum piston alloy using alumina nanoparticles. J Mech Behav Mater. 2023;32(1):20220280.
[19] Kadri E, Krichen M, Mohammed R, Zouari A, Khirouni K. Electrical transport mechanisms in amorphous silicon/crystalline silicon germanium heterojunction solar cell: impact of passivation layer in conversion efficiency. Opt Quantum Electron. 2016;48:1–5.
[20] Al Zubaidi FN, Asaad LM, Alshalal I, Rasheed M. The impact of zirconia nanoparticles on the mechanical characteristics of 7075 aluminum alloy. J Mech Behav Mater. 2023;32(1):20220302.
[21] Kothari R, Kundalwal SI, Sahu SK, Ray MC. Modeling of thermomechanical properties of polymeric hybrid nanocomposites. Polym Compos. 2018;39(11):4148–64.
[22] Kundalwal SI. Review on micromechanics of nano-and micro-fiber reinforced composites. Polym Compos. 2018;39(12):4243–74.
[23] Kundalwal SI, Suresh Kumar R, Ray MC. Effective thermal conductivities of a novel fuzzy fiber-reinforced composite containing wavy carbon nanotubes. J Heat Transf. 2015;137(1):012401.
[24] Liu X, Yin X, Kong L, Li Q, Liu Y, Duan W, et al. Fabrication and electromagnetic interference shielding effectiveness of carbon nanotube reinforced carbon fiber/pyrolytic carbon composites. Carbon. 2014;68:501–10.
[25] Sellam M, Rasheed M, Azizii S, Saidani T. Improving photocatalytic performance: Creation and assessment of nanostructured SnO2 thin films, pure and with nickel doping, using spray pyrolysis. Ceram Int. 2024;50(12):20917–35.
[26] Gupta M, Patil ND, Kundalwal SI. Active damping of multiscale composite shells using Sinus theory incorporated with Murakami's zig-zag function. Thin-Walled Struct. 2023;191:111063.
[27] Gupta M, Ray MC, Patil ND, Kundalwal SI. Effect of orientation of CNTs and piezoelectric fibers on the damping performance of multiscale composite plate. J Intell Mater Syst Struct. 2023;34(2):194–216.
[28] Modanwal RP, Sathiaraj D, Singh PK, Tyagi R, Pazhani A. Role of natural fiber-based composite on wear and friction resistance. In: Tribological aspects of additive manufacturing. United Kingdom: CRC Press; 2024. p. 76–96.
[29] Xie A, Jiang W, Wu F, Dai X, Sun M, Wang Y, et al. Interfacial synthesis of polypyrrole microparticles for effective dissipation of electromagnetic waves. J Appl Phys. 2015;118(20):204105.
[30] Pomposo JA, Rodrıguez J, Grande H. Polypyrrole-based conducting hot melt adhesives for EMI shielding applications. Synth Met. 1999;104(2):107–11.
[31] Yang X, Lu Y. Preparation of polypyrrole-coated silver nanoparticles by one-step UV-induced polymerization. Mater Lett. 2005;59(19–20):2484–7.
[32] Ebrahimi I, Gashti MP. Polypyrrole-MWCNT-Ag composites for electromagnetic shielding: Comparison between chemical deposition and UV-reduction approaches. J Phys Chem Solids. 2018;118:80–7.
[33] Gahlout P, Choudhary V. 5-Sulfoisophthalic acid monolithium salt doped polypyrrole/multiwalled carbon nanotubes composites for EMI shielding application in X-band (8.2–12.4 GHz). J Appl Polym Sci. 2017;134(40):45370.
[34] Cao MS, Song WL, Hou ZL, Wen B, Yuan J. The effects of temperature and frequency on the dielectric properties, electromagnetic interference shielding and microwave-absorption of short carbon fiber/silica composites. Carbon. 2010;48(3):788–96.
[35] Kundalwal SI, Rathi A. Improved mechanical and viscoelastic properties of CNT-composites fabricated using an innovative ultrasonic dual mixing technique. J Mech Behav Mater. 2020;29(1):77–85.
[36] Kundalwal SI, Ray MC. Improved thermoelastic coefficients of a novel short fuzzy fiber-reinforced composite with wavy carbon nanotubes. J Mech Mater Struct. 2014;9(1):1–25.
[37] Gupta M, Ray MC, Patil ND, Kundalwal SI. Dynamic modelling and analysis of smart carbon nanotube-based hybrid composite beams: Analytical and finite element study. Proc Inst Mech Eng Part L J Mater Des Appl. 2021;235(10):2185–206.
[38] Gupta M, Ray MC, Patil ND, Kundalwal SI. Smart damping of a simply supported laminated CNT-based hybrid composite plate using FE approach. Thin-Walled Struct. 2022;171:108782.
[39] Abbasi H, Antunes M, Velasco JI. Recent advances in carbon-based polymer nanocomposites for electromagnetic interference shielding. Prog Mater Sci. 2019;103:319–73.
[40] Dassan EG, Ab Rahman AA, Abidin MS, Akil HM. Carbon nanotube–reinforced polymer composite for electromagnetic interference application: A review. Nanotechnol Rev. 2020;9(1):768–88.
[41] Kundalwal SI, Ray MC. Micromechanical analysis of fuzzy fiber reinforced composites. Int J Mech Mater Des. 2011;7:149–66.
[42] Kundalwal SI, Ray MC, Meguid SA. Shear lag model for regularly staggered short fuzzy fiber reinforced composite. J Appl Mech Trans ASME. 2014;81(9):091001.
[43] Kundalwal SI, Ray MC. Shear lag analysis of a novel short fuzzy fiber-reinforced composite. Acta Mech. 2014;225:2621–43.
[44] Rathi A, Kundalwal SI. Mechanical and fracture behavior of MWCNT/ZrO2/epoxy nanocomposite systems: Experimental and numerical study. Polym Compos. 2020;41(6):2491–507.
[45] Singh PK, Modanwal RP, Kumar D. Fabrication and mechanical characterization of glass fiber/Al2O3 hybrid-epoxy composite. Sadhana. 2021;46(1):32.
[46] Keziz A, Heraiz M, Sahnoune F, Rasheed M. Characterization and mechanisms of the phase's formation evolution in sol-gel derived mullite/cordierite composite. Ceram Int. 2023;49(20):32989–3003.

[47] Bouras D, Rasheed M. Comparison between CrZO and AlZO thin layers and the effect of doping on the lattice properties of zinc oxide. Opt Quantum Electron. 2022;54(12):824.
[48] Liu J, Wan M. Composites of polypyrrole with conducting and ferromagnetic behaviors. J Polym Sci A Polym Chem. 2000;38(15):2734–9.
[49] Grossiord N, Loos J, Van Laake L, Maugey M, Zakri C, Koning CE, et al. High-conductivity polymer nanocomposites obtained by tailoring the characteristics of carbon nanotube fillers. Adv Funct Mater. 2008;18(20):3226–34.
[50] Li C, Thostenson ET, Chou TW. Effect of nanotube waviness on the electrical conductivity of carbon nanotube-based composites. Compos Sci Technol. 2008;68(6):1445–52.
[51] Simien D, Fagan JA, Luo W, Douglas JF, Migler K, Obrzut J. Influence of nanotube length on the optical and conductivity properties of thin single-wall carbon nanotube networks. ACS Nano. 2008;2(9):1879–84.
[52] Li C, Thostenson ET, Chou TW. Dominant role of tunneling resistance in the electrical conductivity of carbon nanotube–based composites. Appl Phys Lett. 2007;91(22):223114.
[53] Keziz A, Rasheed M, Heraiz M, Sahnoune F, Latif A. Structural, morphological, dielectric properties, impedance spectroscopy and electrical modulus of sintered $Al_6Si_2O_{13}$–$Mg_2Al_4Si_5O_{18}$ composite for electronic applications. Ceram Int. 2023;49(23):37423–34.
[54] Jaber AS, Ismael M, Rashid T, Sarhan MA, Rasheed M, Sala IM. Comparesion the electrical parameters of photovoltaic cell using numerical methods. EUREKA: Phys Eng. 2023;27(4):29–39.
[55] Bao WS, Meguid SA, Zhu ZH, Weng GJ. Tunneling resistance and its effect on the electrical conductivity of carbon nanotube nanocomposites. J Appl Phys. 2012;111(9):093726.
[56] Yu Y, Song G, Sun L. Determinant role of tunneling resistance in electrical conductivity of polymer composites reinforced by well dispersed carbon nanotubes. J Appl Phys. 2010;108(8):084319.
[57] Enneffatia M, Rasheed M, Louatia B, Guidaraa K, Shihab S, Barille R. Investigation of structural, morphology, optical properties and electrical transport conduction of Li0. 25Na0. 75CdVO4 compound. IOP Publishing J Phys:Conf Ser. 2021;1795:012050.
[58] Assoudi N, Chaabani A, Rasheed M, Walha I, Dhahri E, Alawsi T, et al. Comparative examination of the physical parameters of the sol gel produced compounds La0. 5Ag0. 1Ca0. 4MnO3 and La0. 6Ca0. 3Ag0. 1MnO3. Opt Quantum Electron. 2022;54(9):556.
[59] Deng F, Zheng QS. An analytical model of effective electrical conductivity of carbon nanotube composites. Appl Phys Lett. 2008;92(7):071902.
[60] Feng C, Jiang L. Micromechanics modeling of the electrical conductivity of carbon nanotube (CNT)–polymer nanocomposites. Compos Part A Appl Sci Manuf. 2013;47:143–9.
[61] Takeda T, Shindo Y, Kuronuma Y, Narita F. Modeling and characterization of the electrical conductivity of carbon nanotube-based polymer composites. Polymer. 2011;52(17):3852–6.
[62] Baxter SC, Robinson CT. Pseudo-percolation: Critical volume fractions and mechanical percolation in polymer nanocomposites. Compos Sci Technol. 2011;71(10):1273–9.
[63] Rasheed M, Shihab S, Alabdali O, Rashid A, Rashid T. Finding roots of nonlinear equation for optoelectronic device. J Phys: Conf Ser. 2021;1999:012077.
[64] Rasheed M, Mohammed OY, Shihab S, Al-Adili A. Explicit numerical model of solar cells to determine current and voltage. J Phys: Conf Ser. 2021;1795:012043.
[65] Dubey P, Gupta M, Pritesh VB, Kundalwal S. Carbon nanotube–based nanocomposite for effective electromagnetic interference shielding in aerospace applications: A finite element study. Finite element analysis of polymers and composites. United States: Woodhead Publishing; 2024. p. 569–97.
[66] Dubey P, Gupta M, Kundalwal SI. Influence of thickness parameter on the EMI shielding effectiveness of CBNC in C-band: A numerical study. Mater Today Proc. 2024;114:7–11.
[67] Dubey P, Gupta M, Kundalwal SI. Conductive polymer nanocomposite incorporated with carbon nanotubes for effective electromagnetic interference shielding: A numerical study. Polym Compos. 2024;45(4):3576–90.
[68] Rohini R, Bose S. Electromagnetic interference shielding materials derived from gelation of multiwall carbon nanotubes in polystyrene/poly (methyl methacrylate) blends. ACS Appl Mater Interfaces. 2014;6(14):11302–10.
[69] Singh P, Kumari R. Monopole patch antenna for C band applications. In TEQIP III Sponsored International Conference on Microwave Integrated Circuits, Photonics and Wireless Networks (IMICPW). IEEE; 2019. p. 333–6.
[70] Rasheed M, Alabdali O, Shihab S, Rashid A, Rashid T. On the solution of nonlinear equation for photovoltaic cell using new iterative algorithms. J Phys: Conf Ser.2021:1999;012078.
[71] Rasheed M, Al-Darraji MN, Shihab S, Rashid A, Rashid T. The numerical calculations of single-diode solar cell modeling parameters. J Phys: Conf Ser. 2021;1963:012058.
[72] Alabdali O, Shihab S, Rasheed M, Rashid T. Orthogonal Boubaker-Turki polynomials algorithm for problems arising in engineering. In AIP Conference Proceedings. USA: AIP publishing; 2022. p. 050019.
[73] Ryvkina N, Tchmutin I, Vilcakova J, Peliskova M, Saha P. The deformation behavior of conductivity in composites where charge carrier transport is by tunneling: theoretical modeling and experimental results. Synth Met. 2005;148(2):141–6.
[74] Wernik JM, Meguid SA. Recent developments in multifunctional nanocomposites using carbon nanotubes. Appl Mech Rev. 2010;63(5):050801.
[75] Taherian R. Experimental and analytical model for the electrical conductivity of polymer-based nanocomposites. Compos Sci Technol. 2016;123:17–31.
[76] Berhan L, Sastry AM. Modeling percolation in high-aspect-ratio fiber systems. I. Soft-core *versus* hard-core models. Phys Rev E - Stat Nonlinear, Soft Matter Phys. 2007;75(4):041120.
[77] Rathi A, Kundalwal SI. Synergistic effect of ultrasonically assisted exfoliated MWCNTs by ZrO2 nanoparticles on thermo-mechanical and anti-corrosive properties of epoxy nanocomposites. J Compos Mater. 2022;56(11):1633–49.
[78] Zare Y, Rhee KY. A simple methodology to predict the tunneling conductivity of polymer/CNT nanocomposites by the roles of tunneling distance, interphase and CNT waviness. RSC Adv. 2017;7(55):34912–21.
[79] Wang Y, Weng GJ. Electrical conductivity of carbon nanotube-and graphene-based nanocomposites. Micromech Nanomech Compos Solids. 2018;123–56.
[80] Tokito S, Tsutsui T, Saito S. Morphology and conductivity of polypyrrole containing halogen counter anions. Chem Lett. 1985;14(4):531–4.
[81] Shi DL, Feng XQ, Huang YY, Hwang KC, Gao H. The effect of nanotube waviness and agglomeration on the elastic property of carbon nanotube-reinforced composites. J Eng Mater Technol. 2004;126(3):250–7.

[82] Rafiee R. Influence of carbon nanotube waviness on the stiffness reduction of CNT/polymer composites. Compos Struct. 2013;97:304–9.
[83] Lu X, Zhang W, Wang C, Wen TC, Wei Y. One-dimensional conducting polymer nanocomposites: Synthesis, properties and applications. Prog Polym Sci. 2011;36(5):671–712.
[84] Lapinsky SE, Easty AC. Electromagnetic interference in critical care. J Crit Care. 2006;21(3):267–70.
[85] Mirmohammadi SA, Sadjadi S, Bahri-Laleh N. Electrical and electromagnetic properties of CNT/polymer composites. In Carbon nanotube-reinforced polymers. Netherlands: Elsevier; 2018. p. 233–58.
[86] Jana PB, Mallick AK, De SK. Effects of sample thickness and fiber aspect ratio on EMI shielding effectiveness of carbon fiber filled polychloroprene composites in the X-band frequency range. IEEE Trans Electromagn Compat. 1992;34(4):478–81.
[87] Al-Saleh MH. Influence of conductive network structure on the EMI shielding and electrical percolation of carbon nanotube/polymer nanocomposites. Synth Met. 2015;205:78–84.
[88] Xu Y, Li Y, Hua W, Zhang A, Bao J. Light-weight silver plating foam and carbon nanotube hybridized epoxy composite foams with exceptional conductivity and electromagnetic shielding property. ACS Appl Mater Interfaces. 2016;8(36):24131–42.
[89] Thomassin JM, Jerome R, Detrembleur C, Molenberg I, Huynen I. Polymer/carbon nanotube composites for electromagnetic interference reduction. In Physical properties and applications of polymer nanocomposites. Woodhead Publishing; 2010. p. 563–87.
[90] Thomassin JM, Pagnoulle C, Bednarz L, Huynen I, Jerome R, Detrembleur C. Foams of polycaprolactone/MWNT nanocomposites for efficient EMI reduction. J Mater Chem. 2008;18(7):792–6.
[91] Chizari K, Arjmand M, Liu Z, Sundararaj U, Therriault D. Three-dimensional printing of highly conductive polymer nanocomposites for EMI shielding applications. Mater Today Commun. 2017;11:112–8.